- Determination of activities and condensation temperatures of GaO<sub>1.5</sub> and InO<sub>1.5</sub> in
- 2 anorthite-diopside eutectic melts by Knudsen Effusion Mass Spectrometry

1

4 Lukas Bischof<sup>1</sup>, Paolo A. Sossi<sup>1,\*</sup>, Dmitry Sergeev<sup>2</sup>, Michael Müller<sup>2</sup>, Max W. Schmidt<sup>1</sup>

5

- 6 <sup>1</sup> Institute of Geochemistry and Petrology, ETH Zürich, CH-8092, Zürich, Switzerland
- <sup>7</sup> IEK-2, Forschungszentrum Jülich, Jülich, Germany
- 8 \* corresponding author. Email address: paolo.sossi@erdw.ethz.ch

9 10

## **Abstract**

1112

13

14

15

16

17

18

19

20

21

22

23

24

25

26

27

28

29

30

31

The group 13 elements Ga and In are overabundant in bulk silicate Earth (BSE) when compared to lithophile elements of similar 50% nebular condensation temperature  $(T_c^{50})$ . To understand whether evaporation from silicate melts provides a more accurate description of volatility during the later stages of planetary accretion, namely, at higher temperatures and oxygen fugacities than in the solar nebula, knowledge of the activities of GaO<sub>1.5</sub> and InO<sub>1.5</sub> in silicate melts and their stable gaseous species are required. To this end, we doped anorthite-diopside (An-Di) eutectic glasses with ~1000 and ~10000 ppm of Ga and In and determined their equilibrium partial pressures above the silicate liquid by Knudsen Effusion Mass Spectrometry (KEMS) using Ir cells at 1550-1740 K over the  $log(fO_2)$  range  $\Delta IW+1.5$  to  $\Delta IW+2.5$  (IW = iron-wüstite buffer). We detect Ga<sup>0</sup> and In<sup>0</sup> as the dominant vapour species and determine activity coefficients of  $\gamma(\text{GaO}_{1.5}) = 0.036(6)$  at 1700 K and of  $\gamma(\text{InO}_{1.5}) = 0.017(12)$  at 1674 K. Using these activity coefficients, we calculate partial pressures of Ga and In, together with those of similarly volatile elements, K and Zn and show that their relative volatilities from Fe- and Na-free basaltic melts are in the in order Ga > K ~ In > Zn, different from those predicted from their  $T_c^{50}$  under nebular conditions but in line with their relative abundances in the BSE. This substantiates the view that the abundances of volatiles in BSE, such as Ga and In, may have been set by evaporation from silicate melts under oxidising conditions at later stages of planetary accretion. Moreover, chondrules likely never underwent significant evaporation during melting and their volatile-depleted nature is likely inherited from the earliest solid condensates.

32 33

Keywords: evaporation, silicate melt, KEMS, Ga, In, activity, accretion

## 1 Introduction

Gallium and indium are moderately and highly volatile elements, respectively, based on their 50% condensation temperatures from a nebular gas with solar composition,  $T_c^{50}$  (Lodders, 2003). Although accurately predicting the  $T_c^{50}$  of Ga and In is difficult given i) the variety of stable gas species in the solar nebula and ii) the uncertainty of their activity coefficients in condensing phases (Fe-metal for Ga and FeS for InS), estimations for their condensation temperatures vary little among different studies. In detail, at  $10^{-4}$  bar, the average  $T_c^{50}(Ga) =$  $993 \pm 66 \text{ K}$  (Lodders, 2003; Wai and Wasson, 1977; Wasson, 1985; Wood et al., 2019) and  $T_c^{50}$ (In) = 495 ± 40 K (Lodders, 2003; Wasson, 1985; Wood et al., 2019) are distinctly resolved. However, the partial pressures and activity coefficients of Ga and In-bearing species are less well constrained for conditions relevant to accreting planets, i.e. at higher temperatures and oxidising conditions where silicate melts are thought to prevail (e.g. O'Neill and Palme, 2008; Visscher and Fegley, 2013; Sossi and Fegley, 2018). Silicate melts may also form at high dust/gas ratios in the solar nebula itself owing to high total pressures (Ebel, 2004), as well as during the formation of chondrules (Libourel and Portail, 2018; Piralla et al., 2021). Therefore, to accurately predict the volatilities of Ga and In during their evaporation from silicate melts, their gas species and the activities of the dissolved components GaO<sub>1.5</sub> and InO<sub>1.5</sub> need to be better understood.

Even though thermodynamic data are available for many gaseous species and modelling of low-pressure gases in the ideal limit is straightforward, there are little data on the mixing properties of moderately- and highly volatile trace elements in silicate melts (Wood and Wade, 2013). Much of the difficulty arises from the proclivity of these elements to evaporate in 1-atm furnaces (*e.g.* O'Neill, 2005; Mathieu *et al.*, 2008, 2011; Sossi *et al.*, 2019; Gellissen et al. 2019; Ni et al. 2021). To ameliorate this problem, such activities are often estimated by examining their partition coefficients,  $D = x_{metal}/x_{silicate}$  (where *x* is the mole fraction) between silicate liquid and Fe-rich metal (Holzheid and Lodders, 2001; Holzheid et al., 1997; O'Neill and Eggins, 2002; O'Neill et al., 2008; Wood and Wade, 2013) in conjunction with the equilibrium constant of reaction. To do so requires accurate estimation of the activity coefficient  $y_{\rm M}$  (where M is the metal of interest) in Fe alloy, which is not always well known. For example, Wood and Wade (2013) deduced a  $y({\rm InO}_{1.5})$  of 0.02 at 1923 K at infinite dilution, by assuming that  $y({\rm In})$  can be treated as a regular solution with Fe, setting the Margules parameter, W, to 52

kJmol<sup>-1</sup> in order to obtain a consolute temperature of 3130 K in the binary Fe-In (where  $T_{consolute}$  = W/2R; Okamoto, 1990). However, the consolute temperature of Okamoto (1990) includes an extrapolation of ~1500 K from experimental data and an assumed composition of Fe<sub>50</sub>In<sub>50</sub>. Moreover, given the lack of an entropy of melting of InO<sub>1.5</sub>, Wood and Wade (2013) had to estimate a value of  $\Delta_{fus}S_{Tm}^{0} = 26.25$  JK<sup>-1</sup> at its melting point,  $T_m$ , of 2183 K, based on that of GaO<sub>1.5</sub> (26.3 JK<sup>-1</sup>). Both assumptions introduce considerable uncertainty and highlight the need for independent estimates of such activity coefficients.

Ko and Park (2011) provide evidence for the existence of  $In^+O_{0.5}$  in CaO-SiO<sub>2</sub>-Al<sub>2</sub>O<sub>3</sub> (CAS) melts at 1773 K and reducing conditions ( $\Delta IW$ -2.6 to  $\Delta IW$ -1.6; IW = iron-wüstite, after the expression of O'Neill and Pownceby, 1993), contrary to the assumption of  $In^{3+}O_{1.5}$  by Wood and Wade (2013). Their assertion is in accord with the change in log(D) vs.  $log(fO_2)$  with oxygen fugacity (from  $\Delta IW$ -1.5 to -4), which yields an oxidation state of 1+ in the silicate melt in equilibrium with Fe-rich alloy (Mann et al., 2009). In their experiments, Ko and Park (2011) heated a silicate slag and pure In metal in a graphite crucible under Ar + CO atmospheres for 12 h at 1773 K. The resulting activity coefficients for  $InO_{0.5}$  vary between  $0.3 \times 10^{-6}$  and  $1.3 \times 10^{-6}$ , depending on silica content (30-80 wt.%), orders of magnitudes lower than the 0.02 for  $InO_{1.5}$  at 1923 K (Wood and Wade, 2013).

Taking into account the uncertainty not only in the activity coefficients, but also in oxidation state of In in silicate melts, as well as the lack of activity data for Ga and In at higher  $fO_2$ , and in melt compositions more relevant to mafic magmatism on planetary bodies, further study is warranted. For this purpose, we use Knudsen Effusion Mass Spectrometry (KEMS), a well-known method for the investigation of thermodynamic properties of chemical substances (*e.g.* Drowart and Goldfinger, 1967; Paule and Margrave, 1967; Drowart *et al.*, 2005; Bischof *et al.*, 2023) and silicate systems (*e.g.* Rammensee and Fraser, 1982; Costa *et al.*, 2017). We identify the gas species evaporating over an anorthite-diopside (An-Di) eutectic liquid containing trace amounts of Ga and In. Comparing equilibrium constants for reactions above this eutectic melt to those above pure sesquioxides of Ga and In (Bischof et al., 2023), activity coefficients,  $\gamma_i$ , of metal oxide components (GaO<sub>1.5</sub>, InO<sub>1.5</sub>) in the silicate melt are calculated. These activity coefficients are compared to  $\gamma_i$  of the group 13 elements B and Al to determine possible trends within the group. Furthermore, volatilities of Ga, K, In and Zn are evaluated at different temperatures T and  $fO_2$ , and used to calculate condensation temperatures from An-Di liquids based on our values of  $\gamma_i$  to illustrate the degree to which these volatilities diverge from those

under solar nebular conditions, and are used to assess the volatile loss history of chondrules attending their formation.

104105

106

103

#### 2 Methods

107 2.1. Sample preparation

108

109 An An-Di eutectic mixture (42 wt.% anorthite and 58 wt.% diopside; nominal composition, in wt. %, of  $SiO_2 = 50.34$ ,  $Al_2O_3 = 15.40$ , MgO = 10.80, CaO = 23.46) was chosen as a compromise 110 111 between achieving a low liquidus temperature (1540 K) whilst still resembling basalt, a composition typical of the Earth's crust and those of small planetary bodies (BSVP, 1981), and, 112 potentially, the late stages of magma oceans (Labrosse et al., 2007; Elkins-Tanton, 2012; 113 Schmidt and Krättli, 2022). This composition was synthesised from reagent-grade SiO<sub>2</sub>, MgO, 114 115 Al<sub>2</sub>O<sub>3</sub> and CaCO<sub>3</sub> homogenised in an agate mortar under acetone. The mixture was decarbonated at 1273 K for 12 h in air, filled into a Pt crucible and placed in a box furnace at 116 117 1673 K for 1 h in air. The melt was quenched to a glass, reground, spiked with 1000 or 10000 ppm of each Ga, In and Tl (added as their sesquioxides), enclosed in an unwelded but crimped 118 119 Pt capsule, heated for 30 min at 1623 K in a vertical tube one-atmosphere gas mixing furnace 120 (ETH Zürich) in air and subsequently quenched. The re-pulverised glass was then used as the 121 starting material for the KEMS experiments. The objective of this procedure is to produce a homogeneous glass starting material, in order to prevent the melt from creeping out of the 122 Knudsen cell and clogging the orifice of its lid during the experiment (cf. section 2.2.1). 123 124 Moreover, as the trace elements are already dissolved in the glass, premature evaporative losses during heating are minimised by reducing the activities of the components relative to the pure 125 126 oxides. Thallium, however, completely evaporated in the subsequent heating process (below ~700 °C) and hence its evaporation could not be further investigated with KEMS. 127

128

- 129 *2.2 Analytical methods*
- 130 2.2.1. Knudsen Effusion Mass Spectrometry (KEMS)

131132

133

134

135

136

Experiments were carried out with a FINNIGAN MAT 271 Knudsen effusion mass spectrometer at Forschungszentrum, Jülich. For a detailed description of the instrument and methodology, the reader is referred to Bischof *et al.* (2023). Briefly, the iridium Knudsen cell (KC) is composed of a crucible 8.5 mm high with an outer diameter of 7.8 mm and 0.2 mm wall thickness, and a lid with a 0.4 mm orifice at its centre. The KC is contained in W housing and

is heated by a W wire, whose temperature is monitored by a W<sub>97</sub>Re<sub>3</sub>/W<sub>75</sub>Re<sub>25</sub> thermocouple, while the temperature at the Ir cell is determined using a single wavelength pyrometer (IGA-12, LUMASENSE TECHNOLOGIES). The entirely assembly is surrounded by three nested Ta heatshields. Heating was achieved by means of a W wire and radiative heating below ~600 °C and electron bombardment above this temperature. The KC chamber (~10<sup>-6</sup> mbar) can be isolated through a shutter from all other compartments of the device (~10<sup>-9</sup> mbar), enabling determination of sample- (shutter open) and background (shutter closed) signals. Ionisation of the molecular beam effusing from the KC is achieved by electron impact. Ions are accelerated towards the entrance slit of the mass spectrometer by an electrical potential of 6 kV. The resulting signal intensity of the ions was determined using an ion-counter.

To avoid contamination and to anneal the cell material, empty iridium KCs were heated to 1930 K for 12 h. Powdered glasses, 40 mg for the runs with high trace elements concentrations and 80 mg for the runs with low trace element concentrations, were then packed into the KC and heated to ~973 K. Following mass scans from 10 amu to 250 amu for the analysis of vapour species above the sample, the spatial position of the KC was optimised to achieve the highest signal sensitivity. These scans also revealed the presence of WO<sub>3</sub><sup>+</sup> and WO<sub>2</sub><sup>+</sup>, as well as minor Mg<sup>+</sup> and Na<sup>+</sup> in the mass spectrum at high temperatures. Their intensities were outweighed by those of Ga- and In-bearing species, indicating that these are the main constituents of the high temperature vapour above the silicate melt.

Given an electron ionisation energy  $E(e^-)$  of 60 eV and a constant electron emission  $i_{(em)}$  of 0.468 mA, the intensity of each species (Table 1) was measured over a 1% mass window of its nominal mass, a scan consisting of 301 steps and a counting time of 0.1 s/step. The measurement protocols used were *isotherm* or *polytherm*. The former refers to measuring ion intensities at a constant temperature over a given duration, whereas the latter involves measurement at discrete temperature steps. Detected species and their respective mass-to-charge ratios (m/z) are summarised in Table 1, measurement conditions are given in Table 2, and full results in Supplementary Material Tables S1 – S4.

Table 1: Masses and isotopic abundances of the measured ions. The ions listed concern only those whose intensities were measured; other ions, whose intensities were not recorded, may also be present.

Ga In

Species	m/z	Isotopic	Species	m/z	Isotopic
		abundance			abundance
		[%]			[%]
Ga <sup>+</sup>	69	60.1	In <sup>+</sup>	115	95.7
				113	4.3
${\rm GaO}^+$	85	60.0	$InO^{+}$	131	95.5
$\mathrm{Ga}_2^+$	138	36.1	$In_2^+$	230	91.6
				228	8.4
$\mathrm{Ga_2O}^+$	156	47.9	$In_2O^+$	246	91.4
$\mathrm{Ga_2O}^+$ $\mathrm{O_2}^+$	32	99.5	${\rm O_2}^+$	32	99.5

Table 2: Samples, their weights and measurement parameters in isotherm and polytherm runs. The ions listed concern only those whose intensities were measured; other ions, whose intensities were not recorded, may also be present.

Run	Initial weight [mg]	Final weight [mg]	Isotherm parameters		Polytherm parameters			Ions measured	
			<i>T</i> [K]	t [h]	T range [K]	T step [K]	Equili- bration time	Ramp	-
							[min]		
1_low, initially	79.1	79.1	1742	15	1585-	10	5	up	Ga <sup>+</sup> ; GaO <sup>+</sup> ;
1000 ppm					1695				$Ga_2^+; Ga_2O^+;$
2_low, initially	72.92	71.97	-	-	1400-	10	5	up	In <sup>+</sup> ; InO <sup>+</sup> ;
1000 ppm					1730				$In_2^+; In_2O^+;$
3_high, initially 10000 ppm	38.69	38.69	-	-	1540- 1640	10	5	up	$\mathrm{O}_2^+$

# 2.2.2. Electron probe micro-analyser (EPMA)

The mass fractions of the main components SiO<sub>2</sub>, Al<sub>2</sub>O<sub>3</sub>, MgO and CaO were determined in the starting (pre-KEMS) and residual glasses (post-KEMS; KC is cut lengthwise; *cf.* Supplementary Material, Fig. S1) using a JEOL-JXA 8200 electron probe micro-analyser (EPMA) equipped with 5 wavelength dispersive spectrometers (ETH Zürich). Measurements were made at an accelerating voltage of 15 kV, a beam current of 20 nA, a beam diameter of 20 µm and peak counting times of 20 s for Si, Al and Mg, and of 40 s for Ca. We used the

crystals TAP for Al, Mg and Si, and PETJ for Ca and the standards albite (NaAlSi<sub>3</sub>O<sub>8</sub>) for Si, anorthite (CaAl<sub>2</sub>Si<sub>2</sub>O<sub>8</sub>) for Al and Ca, wollastonite (CaSiO<sub>3</sub>) for Ca, corundum for Al, forsterite (Mg<sub>2</sub>SiO<sub>4</sub>) and periclase (MgO) for Mg. Mean atomic number background intensities were calibrated and continuum absorption corrected according to Donovan and Tingle (1996) and Donovan *et al.* (2016), while the matrix correction method used was ZAF or Phi-Rho-Z calculations (Armstrong, 1988). Oxygen was calculated by cation stoichiometry and included in the matrix correction.

2.2.3. Laser ablation inductively coupled plasma-mass spectrometry (LA-ICP-MS)

The concentrations of Ga and In in the starting and post-KEMS glasses (KC is cut lengthwise; cf. Supplementary Material, Fig. S2) were determined by means of a ASI Resolution 193 nm ArF excimer laser paired with a LAURIN Technic 155 constant geometry 2-volume ablation cell, coupled to a Thermo Element XR sector-field ICP-MS at ETH Zürich (Guillong et al., 2014). Measurements used a spot size of 29 µm, a repetition rate of 4.60 Hz, laser energy of 3.5 J/cm<sup>2</sup>, an acquisition time of 30 s for each ablation and background, and an analysis time per element of 0.455 s. Laser spots were placed as traverses across the entire glass (Supplementary Material, Fig. S2) to check for spatial heterogeneity. We used NIST-610 as the external standard, and BCR-2G and GSD-2G as secondary standards to monitor data quality in matrices similar to those of the An-Di glasses. Raw data were processed using the IOLITE software (Woodhead et 

al., 2007; Paton et al., 2011) with Si as the internal standard element.

- **3 Theoretical framework**
- *3.1. Determination of partial pressures*

209 Partial pressures of the species under consideration are calculated based on the ion intensities 210 determined by KEMS (eq. 1):

$$p_i = \frac{kI_iTf_{M^+}}{\eta_i\gamma_{m,i}\sigma_i}. (1)$$

Here,  $p_i$  describes the partial pressure of species i, k the instrument sensitivity factor,  $I_i$  the measured intensity of the respective ion, T the temperature in the KC (in K),  $f_{M^+}$  the

fragmentation correction based on the ratio of M<sup>+</sup> to  $\Sigma$ M<sup>+</sup> with values between 0 and 1,  $\eta_i$  the isotopic abundance of species i,  $\gamma_{m,i}$  the multiplier factor of species i and  $\sigma_i$  the ionisation cross section of species i. The process of deriving partial pressures from measured intensities is described in full in Bischof *et al.* (2023), only the most pertinent aspects are discussed here.

Gaussian fits to the intensity of the isotope in each mass scan were performed to determine  $I_i$ . The associated error,  $\Delta I_i$  calculated from the fitting procedure is ~0.25% of the measured value. The isotopic abundance  $\eta_i$  is 0.60 for <sup>69</sup>Ga, 0.96 for <sup>115</sup>In and 0.99 for <sup>16</sup>O (*cf.* Table 1). Where there are several isotopologues (*e.g.* <sup>69</sup>Ga<sup>69</sup>Ga, <sup>69</sup>Ga<sup>71</sup>Ga, <sup>71</sup>Ga<sup>71</sup>Ga), the most abundant was measured. Their relative intensities are shown to be within error of those of expected from natural abundances of Ga and In isotopes, affirming that there is a negligible contribution to their intensities from any potential isobars. The error of the isotopic abundances  $\Delta \eta_i$  is negligible for our purposes.

The determination of the instrument sensitivity factor k as well as temperature calibration were carried out before and after sample measurements *in-situ* by measuring i) the melting points,  $T_m$ , of pure Ag (1235 K) and Ni (1728 K) and ii) the counts of Ag<sup>+</sup> and Ni<sup>+</sup> at  $T_m$ . Based on Bischof *et al.* (2023), with measurements performed in the same analytical session, the instrument sensitivity factor k and the real temperature  $T_{real}$  are determined as (eqs. 2 and 3)

$$k = 1.52(6) \times 10^{-7} \times T_{pyr} + 2.9(6) \times 10^{-5}$$
 (2)

$$T_{real} = 1.060(4) \times T_{pvr} + 53(4) \tag{3}$$

where  $T_{pyr}$  is measured by pyrometry with an error of  $\pm 5$  K. The multiplier factor  $\gamma_{m,i}$  is set to 1 (hence  $\Delta \gamma_{m,i} = 0$ ), as intensities were determined with an ion counter (Bischof et al., 2023). The ionisation cross sections used for the individual species,  $\sigma_i$ , as well as their errors are summarised in Table 3. The cross section of oxygen  $\sigma(O_2) = 2.8$  is taken from Fite and Brackmann (1959), its error of 17% (= 0.5) is estimated based on that of the other cross sections.

Table 3: Summary of ionisation cross sections of measured species (Bischof et al., 2023).

Ga	1	In		
Species	$\sigma_i  [\mathring{ m A}^2]$	Species	$\sigma_i  [\mathring{ m A}^2]$	

Ga <sup>+</sup>	$7.96 \pm 1.38$	In <sup>+</sup>	$9.74 \pm 1.48$
$\mathrm{GaO}^+$	$6.24\pm1.35$	$InO^+$	$7.50\pm1.45$
$\mathrm{Ga}_2^+$	$11.94\pm1.97$	$In_2^+$	$14.61 \pm 2.09$
$\mathrm{Ga_2O}^+$	$13.20\pm2.08$	$In_2O^+$	$16.03\pm2.22$

Ionisation efficiency curves above pure  $Ga_2O_3(s)$  and  $In_2O_3(s)$ , constructed by measuring the intensity of a given gas species while scanning the ionising energy of the incoming electrons from 0 to 60 eV, exhibit clear indications for fragmentation of molecular gas species into smaller constituents via electron-impact. That is, the intensity of the signal measured for a particular ion (*e.g.* M<sup>+</sup>) may not derive only from M<sup>0</sup>, but also contain contributions from different polyatomic molecules, such as  $M_2O^0$  (Bischof et al., 2023; Gomez et al., 1982; Smirnov et al., 2021). Hence, a correction factor  $f_{M^+}$  is introduced, which is calculated as an ion current  $i_i$  ratio at the ionising energy of 60 eV for pure oxides (eq. 4):

$$f_{\rm M^+} = \frac{i_{\rm M^+, 60 \, eV}}{i_{\rm M^+, 60 \, eV} + i_{\rm M_2O^+, 60 \, eV}}.$$
 (4)

Adding Ga and In in trace amounts (initially 1000 and 10000 ppm) changes the  $M_2O^+/M^+$  ratio of the vapour relative to that above the pure oxides and therefore the ion current of  $M_2O^+$ ,  $i_{M_2O^+, 60 \text{ eV}}$ , has to be corrected accordingly. This is carried out by multiplication of the initial value for the ion current of  $M_2O^+$ ,  $i_{M_2O^+, 60 \text{ eV}}$ ,  $i_{nit}$ , taken from the ionisation efficiency curves in Bischof *et al.* (2023) with the intensity ratios of  $M_2O^+/M^+$  above the An-Di eutectic melt or the pure oxides, respectively (eq. 5)

$$i_{\text{M}_2\text{O}^+, 60 \text{ eV}} = i_{\text{M}_2\text{O}^+, 60 \text{ eV}, init.} \times \frac{\frac{I_{\text{M}_2\text{O}^+, \text{An-Di}}}{I_{\text{M}^+, \text{An-Di}}}}{\frac{I_{\text{M}_2\text{O}^+, \text{p.o.}}}{I_{\text{M}^+, \text{p.o.}}}}.$$
 (5)

Here,  $I_{i, \text{An-Di}}$  is the measured intensity of a species above the An-Di eutectic melt and  $I_{i, p.o.}$  that above pure oxides (taken from Bischof et al., 2023).

Table 4: Summary of quantities used for the calculation of  $f_i$ .

Element	Ga	In	In	
$i_{\rm M_2O^+,\ 60\ eV,\ orig.}[\%]$	45.90 <sup>1)</sup>	40.52 1)		

$f_{M^+}$	0.18	0.26	
$i_{M^+, 60 \mathrm{eV}}  [\%]$	7.48 1)	9.61 1)	
$I_{\mathrm{M}^{+},\mathrm{p.o.}}[\mathrm{cps}]$	21462 4)	605097 <sup>5)</sup>	
$I_{\rm M_2O^+,\ p.o.}$ [cps]	1668 <sup>4)</sup>	46669 <sup>5)</sup>	
$I_{\mathrm{M^+, An-Di}}$ [cps]	287 <sup>2)</sup>	2969 <sup>3)</sup>	
$I_{\rm M_2O^+,\ An-Di}$ [cps]	16 <sup>2)</sup>	152 <sup>3)</sup>	

<sup>1)</sup> Bischof *et al.* (2023)

The correction factor  $f_{M^+}$  is multiplied by the intensity measured for  $M^+$  to remove the apparent contribution from the fragmentation of  $M_2O^0$ . To obtain p(M), the intensity of  $M^+$ , reflecting that solely from ionisation of  $M^0$ , is multiplied by the ionisation cross section of  $M^+$  according to eq. 1 (*cf.* Bischof *et al.* 2023). The correction for the partial pressures  $p_i$  of  $M_2O$  is carried out analogously to the experiments above pure oxides (eq. 6, Bischof et al. 2023),

$$p_{M_2O, corr.} = p_{M_2O, init.} + (p_{M, init.} \times (1 - f_{M^+}))$$
 (6)

where  $p_{M_2O,\ corr.}$  is the corrected partial pressure and 'init.' refers to the initial partial pressure calculated from the specific ion intensity assuming  $f_{M_2O^+}=1$ . In run 3\_high,  $f_{M^+}$  is found to be 0.18 (Ga<sup>+</sup>) and 0.26 (In<sup>+</sup>) (eq. 5; Table 4). Since there is no or little  $M_2O^+$  detected in runs 1\_low and 2\_low,  $f_{M^+}=1$  for both Ga<sup>+</sup> and In<sup>+</sup> for these runs, that is, all M<sup>+</sup> is assumed to originate from M<sup>0</sup> and not from fragmentation of  $M_2O^0$  and hence no correction is applied. The error of the correction factor  $f_{M^+}$ ,  $\Delta f_{M^+}$ , is 0.1 for all species, based on the accuracy and precision of the ionisation efficiency curves (Bischof et al., 2023). Doubly- and triply-charged Ga and In were detected, however, their relative proportions were lower (~22 % and 5 %, respectively; Bischof et al. 2023) than those for Ga<sup>+</sup> and In<sup>+</sup>. Moreover, as the instrument sensitivity factor is calibrated on the intensities of the singly-charged ions only (Ni<sup>+</sup> and Ag<sup>+</sup>), the intensities of  $M^{2+}$  and  $M^{3+}$  were not measured in the present study.

 $<sup>^{2)}</sup>$  run 3 high at T = 1598 K

 $<sup>^{3)}</sup>$  run 3 high, average of the intensities at T = 1539 K and T = 1547 K

<sup>&</sup>lt;sup>4)</sup> Bischof *et al.* (2023) at T = 1598 K

<sup>&</sup>lt;sup>5)</sup> Bischof *et al.* (2023) average of the intensities at T = 1535 K and T = 1548 K

High background signals of  $O_2$  are the result of heating of the W container external to the Ir KC, leading to the production of  $WO_3(g)$  and  $WO_2(g)$  throughout the measurements. As the W container is not in contact with the silicate liquid, the  $O_2^+$  signal measured does not reflect that intrinsic to the evaporation of the liquid. This observation, together with the barely resolvable signal of  $O_2^+$  relative to the background, means that its partial pressure is not readily obtained by measured intensities, but by stoichiometry (Bischof et al., 2023; Copland and Jacobson, 2010; Kobertz et al., 2014). That is, the total partial pressure of oxygen is calculated from the sum of the partial oxygen pressures generated in dissociative vaporisation reactions at the melt surface. The gaseous phase above our melt, in addition to Ga and In, also contains SiO and Mg. Although  $Al_2O_3$  and CaO are also major components, the low partial pressures of their gas species contribute minimally to  $O_2$  in the gas phase (e.g. Sossi and Fegley, 2018; and references therein). In this work, the corresponding ion intensities of the SiO<sup>+</sup> and Mg<sup>+</sup> were not measured, and instead their partial pressures were calculated according to their two major vaporisation reactions (eqs. 7 and 8);

$$SiO_2(1) = SiO(g) + 0.5 O_2(g)$$
 (7)

$$MgO(1) = Mg(g) + 0.5 O_2(g)$$
 (8)

and their partial pressures (eqs. 9 and 10)

$$p(SiO) = \frac{K_{(7)} a(SiO_2) p^0}{\left(\frac{p(O_2)}{p^0}\right)^{0.5}}$$
(9)

$$p(Mg) = \frac{K_{(8)} a(MgO) p^{0}}{\left(\frac{p(O_{2})}{n^{0}}\right)^{0.5}}$$
(10)

with  $K_{(7),(8)}$  the equilibrium constant of the respective reaction,  $a_i$  the activity of a species i and  $p^0$  as standard state partial pressure of 101325 Pa. Taking Gibbs free energy of formation  $\Delta_f G_T^0$  given in literature (Chase, 1998),  $K_{(7),(8)}$  for both reactions is calculated as (eqs. 11 and 12),

$$\Delta_r G_T^0 = \sum \Delta_f G_T^0(products) - \sum \Delta_f G_T^0(reactants)$$
 (11)

$$K_{(7),(8)} = \exp\left(-\frac{\Delta_r G_T^{0}(i)}{RT}\right) \tag{12}$$

where  $\Delta_r G_T^0$  is the Gibbs free energy of reaction and R the universal gas constant. Fitting the results as  $1/T vs. \ln(K_{(7),(8)})$  leads to (eqs. 13 and 14),

$$\ln(K_{(7)}) = -\frac{95666(119)}{T} + 29.7(2) \tag{13}$$

$$\ln(K_{(8)}) = -\frac{81507(43)}{T} + 23.70(8) \tag{14}$$

- the errors given in parentheses resulting from the fitting procedure. Activities  $a_i$  for SiO<sub>2</sub> and
- 320 MgO in the An-Di melt are calculated by (eq. 15)

$$a_i = x_i \, \gamma_i \tag{15}$$

- with  $x_i$ , the mole fraction of a species i is 0.497 for SiO<sub>2</sub> and 0.157 for MgO (Table 6). The
- activity coefficients,  $\gamma_i$ , are calculated for the liquid melt oxide components SiO<sub>2</sub> and MgO using
- 325 the MELTS/VapoRock code (Wolf et al., 2023), yielding  $\gamma(SiO_2) = 0.66 0.64$  and  $\gamma(MgO) =$
- 0.03 0.09 at 1389 1740 K. From eqs. 7 and 8, the oxygen partial pressure  $p(O_2)$  must be half
- 327 the sum of p(SiO) and p(Mg) (eq. 16)

$$p(O_2) = \frac{(p(SiO) + p(Mg))}{2}.$$
 (16)

Therefore,  $p(O_2)$  can be determined by solving eqs. 9, 10 and 16 simultaneously minimising the misfit by least-squares. The  $pO_2$  calculated according to eq. (16) agrees to within 0.07 log units relative to that returned by the Slag-Liq model of FactSage and to within 0.15 log units compared to MAGMA throughout the temperature range 1389 – 1740 K, translating to differences in the deduced  $\gamma_i$  of <15 % relative. Trace fractions of Fe and Na that may be present in the gas phase were not included in the calculation of  $pO_2$ . Their evaporation from 500 ppm of FeO or 100 ppm NaO<sub>0.5</sub> dissolved in the liquid would shift the  $pO_2$  given by eq. (16) by 4 % relative, and are thus ignored. The partial pressures of oxygen generated from the vaporisation reactions of  $GaO_{1.5}(1)$  and  $InO_{1.5}(1)$  are calculated according to the partial pressures of the species released within these reactions, *i.e.* p(M), p(MO),  $p(M_2)$  and  $p(M_2O)$ , directly measured *via* KEMS as derived in Bischof et al. (2023) (Table 5). The coefficients equal the

stoichiometric coefficients for the reaction multiplied by a transmission efficiency factor from the KC related to the inverse square root of their masses, for example,  $pO_2(^{69}Ga) = 0.75 \times [(m^{32}O_2)/(m^{69}Ga)]^{0.5} = 0.51$  (Copland and Jacobson, 2010; Kobertz et al., 2014).

Table 5: Summary of equations for the calculation of  $p(O_2)$ .

p(O <sub>2</sub> ) derived from species	Equation
$p_{\mathrm{Ga}}(\mathrm{O}_2)$	0.51 <i>p</i> (Ga)
$p_{ m GaO}({ m O}_2)$	0.15 p(GaO)
$p_{ m Ga2O}({ m O}_2)$	$0.45 p(Ga_2O)$
$p_{ m In}({ m O}_2)$	0.40  p(In)
$p_{ m InO}({ m O}_2)$	0.12 <i>p</i> (InO)
$P_{ m In2O}({ m O}_2)$	0.36 p(In <sub>2</sub> O)

The total partial pressure of oxygen  $p(O_2)$  is subsequently obtained as sum of the partial pressures of the different vaporisation reactions (eq. 17).

$$p(O_2) = p_{SiO}(O_2) + p_{Mg}(O_2) + p_{M}(O_2) + p_{MO}(O_2) + p_{M_2}(O_2) + p_{M_2O}(O_2)$$
(17)

# 3.2. Determination of activity coefficients of melt oxide species

For the calculation of activity coefficients of MO<sub>1.5</sub>, equilibrium constants for the reaction  $MO_{1.5}(l) = M(g) + 0.75 O_2(g)$ , where M = Ga or In, above pure oxides  $(K_{p.o.})$  and above An-Di eutectic  $(K_{An-Di})$  have to be determined. Bischof *et al.* (2023) determined the vaporisation reactions occurring above pure  $Ga_2O_3(s)$  and  $In_2O_3(s)$ . Hence, to calculate  $\gamma(MO_{1.5}(l))$  for the liquid phase,  $K_{p.o.}$  has to be corrected by the enthalpy of fusion at the melting point of  $M_2O_3(s)$ . The Gibbs free energy of fusion  $\Delta_{fus}G_T^0$  can be estimated (eq. 20; Sossi and Fegley, 2018);

$$\Delta_{\text{fus}}G_T^{\text{o}} = \left(\frac{\Delta_{\text{fus}}H_{T_{\text{m}}}^{\text{o}}}{T} - \Delta_{\text{fus}}S_{T_{\text{m}}}^{\text{o}}\right) \times T = \left(\frac{\Delta_{\text{fus}}H_{T_{\text{m}}}^{\text{o}}}{T} - \frac{\Delta_{\text{fus}}H_{T_{\text{m}}}^{\text{o}}}{T_{\text{m}}}\right) \times T,\tag{18}$$

where  $T_{\rm m}$  is the melting point,  $\Delta_{\rm fus}S_{T_{\rm m}}^{\rm o}$  the entropy of fusion and  $\Delta_{\rm fus}H_{T_{\rm m}}^{\rm o}$  the enthalpy of fusion, both at the melting point,  $T_{\rm m}$ . The Gibbs free energy of fusion  $\Delta_{\rm fus}G_T^{\rm o}$  is added to obtain  $\Delta_{r}G_{T_{\rm m}}^{\rm o}$  (eq. 21),

$$\Delta_r G_{T, (1-g)}^0 = \Delta_r G_{T, (s-g)}^0 + \Delta_{\text{fus}} G_T^0. \tag{19}$$

Following this correction for the free energy associated with fusion, expressions for  $K_{\text{p.o.}}$  of the solids given in Bischof *et al.* (2023) can be corrected for the free energy relative to the liquid state, yielding, for M = Ga (eq. 20),

367

$$K_{p.o.}^{GaO_{1.5}(l)} = \exp(-112079(1059)/T + 40.3(7))$$
 (20)

368

369 and for M = In (eq. 21),

$$K_{n.o.}^{InO_{1.5}(l)} = \exp(-90606(682)/T + 33.1(6)).$$
 (21)

370

- Above the silicate melt,  $K_{\text{An-Di}}$  is determined from the partial pressures of p(M) and  $p(O_2)$
- according to (eq. 22),

373

$$K_{\text{An-Di}} = \frac{\left(\frac{p(M)}{p^0}\right) \left(\frac{p(O_2)}{p^0}\right)^{0.75}}{x_{\text{An-Di}}(MO_{1.5})\gamma_{\text{An-Di}}(MO_{1.5})}.$$
 (22)

374

Here,  $x_{\text{An-Di}}(\text{MO}_{1.5})$  is obtained from LA-ICP-MS, leaving  $y_{\text{An-Di}}(\text{MO}_{1.5})$  as the unknown quantity, calculated from (eq. 23)

377

$$\gamma_{i,\text{An-Di}} = \frac{K_{\text{An-Di}}}{K_{\text{p.o.}}}.$$
 (23)

378

**4 Results** 

4.1. EPMA

380

- 382 Abundances of the main components of the glasses were determined before and after the KEMS
- 383 experiments via EPMA (Supplementary Material, Tables S5 S9). In addition to arbitrarily
- spread measurement points, profiles were taken from the inner part to the surface of the glasses
- (cf. Supplementary Material, Fig. S6 S10) to determine compositional variability within the
- samples. Concentrations exhibit a variability of up to ~0.5 wt.% for SiO<sub>2</sub>, ~0.4 wt.% for Al<sub>2</sub>O<sub>3</sub>
- and ~0.3 wt.% for MgO, but no statistically significant spatial trends in the abundances of these
- oxides are identified. In contrast, we find marginally increasing CaO towards the surface of up

to  $\sim$ 0.7 wt.%. Trace quantities of Ti ( $\sim$ 100 ppm) and Fe ( $\sim$ 500 ppm) are observed in the 1\_low composition (see Supplementary Material, Table S1). Totals are lower ( $\sim$ 98.5 %) in the 3\_high composition glasses, owing to the fact that they contain  $\sim$ 1.1 wt. % and  $\sim$ 0.2 wt. % of Ga<sub>2</sub>O<sub>3</sub> and In<sub>2</sub>O<sub>3</sub>, respectively. Average mass fractions are summarised in Table 6.

Table 6: Summary of the results from EPMA. 'Start' denotes the starting glass material pre-experiment, while 'End' indicates the composition post-KEMS experiment.

Sample 1_low		ow	2_1	low	3_l	nigh
Mass fraction [wt.%]	Start	End	Start	End	Start	End
SiO <sub>2</sub>	$50.47 \pm 0.09$	$50.60 \pm 0.18$	$50.47 \pm 0.09$	$50.46 \pm 0.17$	$49.72\pm0.09$	$49.92 \pm 0.39$
$Al_2O_3$	$15.38 \pm 0.08$	$15.31 \pm 0.09$	$15.38 \pm 0.08$	$15.48 \pm 0.07$	$15.15\pm0.08$	$15.22 \pm 0.12$
MgO	$10.42\pm0.04$	$10.38 \pm 0.10$	$10.42\pm0.04$	$10.72 \pm 0.08$	$10.27 \pm 0.04$	$10.70 \pm 0.07$
CaO	$23.63\pm0.09$	$23.65 \pm 0.27$	$23.63 \pm 0.09$	$23.25 \pm 0.05$	$23.28 \pm 0.09$	$22.98 \pm 0.08$
Total	$99.90 \pm 0.16$	$99.94 \pm 0.35$	$99.90 \pm 0.16$	$99.91 \pm 0.21$	$98.42 \pm 0.16$	$98.82 \pm 0.42$

## 4.2. LA-ICP-MS

The amount of Ga and In dissolved in the An-Di glass was determined prior to and after the KEMS experiments using LA-ICP-MS (*cf.* Supplementary Material, Tables S2 – S6, Fig. S7, S8). The concentration measured at the surface is the most representative of the equilibrium concentration at the time of the highest temperature KEMS measurements (after which the samples were quenched). Hence, the chemical profiles measured in the glasses should represent those of the melts at the experimental temperature. The amount of Ga (Supplementary Material, Fig. S7) is constant within uncertainty (~3% relative) across linear profiles for all glasses. All profiles exhibit a significant decrease in In concentration towards the surface. We find relative decreases between the interior and the surface of 48-83% (Supplementary Material, Fig. S8). Concentrations of Ga and In in each glass are listed in Table 7.

Table 7: Summary of the results from LA-ICP-MS analysis.

Sample	Ga In					
	Start	End	Start	End		
	Amoun	t [ppm]	Amount [ppm]			
				Min.	Max.	
1_low	$720 \pm 12$	429 ± 9	47 ± 9	$0.0065 \pm 0.0043$	$0.05 \pm 0.01$	
2_low	$720\pm12$	$695\pm22$	$47\pm 9$	$0.14 \pm 0.01$	$0.85 \pm 0.02$	

3 high  $7185 \pm 618$   $7998 \pm 73$   $5296 \pm 560$   $890 \pm 7$   $1715 \pm 12$ 

Comparing absolute concentrations in the 'low' and 'high' glasses (nominal concentrations of Ga and In of 1000 and 10000 ppm, respectively), it becomes apparent that preparation of the starting glasses led to significant losses of Ga (~28% for all runs) and In (~95% and ~47% for runs with low and high trace element concentrations, respectively). The large standard deviations in the concentrations of the starting material for run 3\_high is due to variations in concentration of the glass fragments analysed, which range between 6370 ppm and 7960 ppm for Ga and 4560 ppm and 5920 ppm for In. However, as the samples were loaded into the KC as powders, and activity determinations are made using concentrations in the glass post-experiment, starting sample inhomogeneity is of little consequence for our purposes. Gallium concentrations during runs 2\_low and 3\_high remained constant within uncertainty, while run 1\_low lost ~40% of its Ga, a consequence of the polytherm run being followed by an isotherm of 15 h, 1742 K (Table 2). The Ga concentration in the glass of run 3\_high is nominally higher than the average initially determined, but not statistically significant, as the RSD (~8%) is higher than the measurement precision (~2-3%). For In, concentrations of the glass after each KEMS run decrease by 83 to 99% relative to that in the starting glass.

## 4.3. KEMS - Isotherm

In order to assess whether the sensitivity of the instrument and the relative abundances of vapour species change within the course of a measurement, and hence to determine the timescale required for the system to reach thermal equilibrium inside the KC, an isotherm was run for 15 h at 1742 K with one measurement of ion intensity per hour, directly following the polytherm run 1\_low (Supplementary Material, Table 2, Fig. 1).

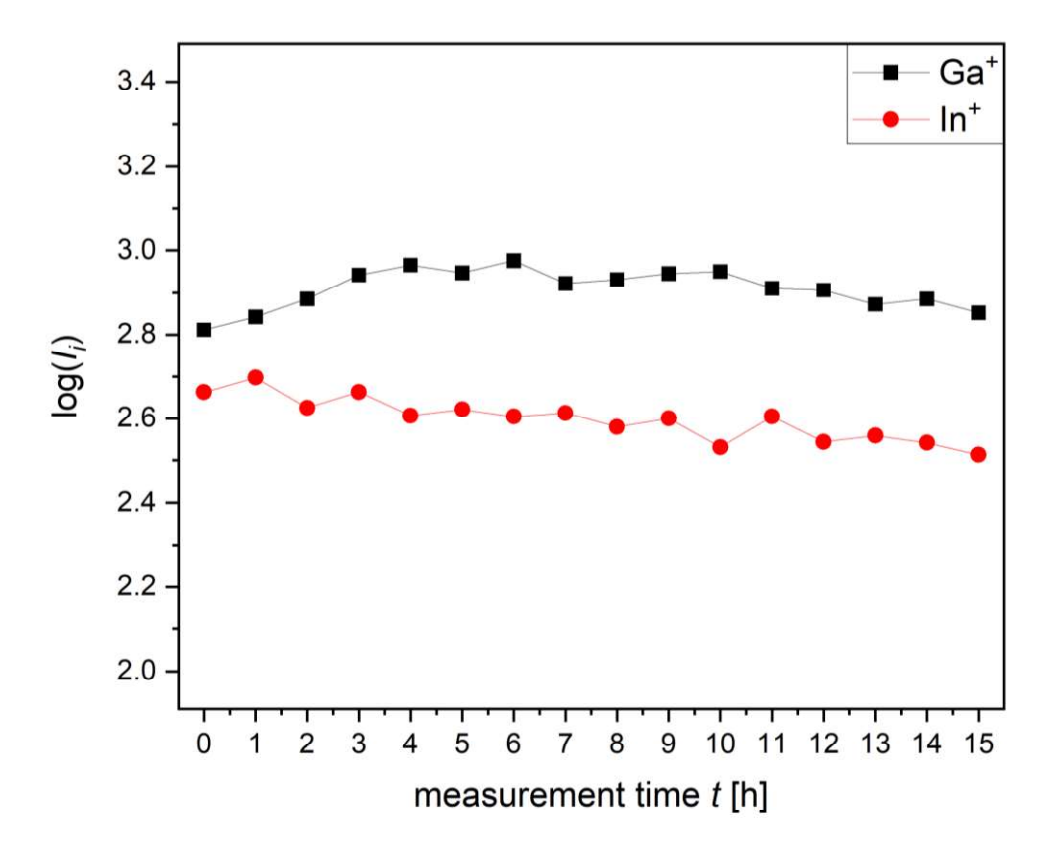


Fig. 1: Isotherm measurement at 1742 K for 15 h, reported are the main trace element species Ga<sup>+</sup> and In<sup>+</sup>.

Intensities are near-constant for Ga (an initial 31 % increase before decreasing slowly by 25% after 15 h) while they decrease for In (~34%) over 15 h. This increase in Ga<sup>+</sup> intensity is sympathetic to a decrease in that of In<sup>+</sup>. Isotherm measurements of pure  $Ga_2O_3(s)$  in the same analytical session show that the intensities of  $Ga^+$  vary by, at most, 3 % relative over a 12 h period at 1622 K (Bischof *et al.* 2023). Hence, the factor ~10 greater increase observed here (Fig. 1) is likely instead due to changes in the  $fO_2$  above the sample induced by the progressive loss of In. In order to augment  $Ga^+$  intensity by 31 % whilst keeping temperature and  $aGaO_{1.5}$  constant, an 8 % relative decrease in  $fO_2$  is required (as pGa is proportional to  $fO_2^{-3/4}$ , eq. 22). The vaporisation of In contributes to ~5 % of the  $fO_2$  above the anorthite-diopside eutectic liquid in the isotherm run at 1740 K; a similar order of magnitude to that required. Owing to zoning of In observed in the glasses, the exact amount of In loss is difficult to quantify. Nevertheless, this degree of In loss is the most likely explanation of the relative increase in  $Ga^+$ , despite an overall decrease in its concentration in the melt during the 1\_low experiment (Table 7).

Given that one measurement in a polytherm run takes  $\sim 15$  min (5 min of equilibration to a new temperature, 10 min measurement of the different species), we divide the largest intensity difference between two measurements in the isotherm run (1 hour) by 4 to obtain  $dI/dt \sim 28$ 

cps/15 min (~3%). For p(Ga) at 1733 K, a dI/dt of 28 cps/15 min corresponds to  $\Delta p(Ga) = 3.77 \times 10^{-5}$  Pa, which is an order of magnitude lower than the error of  $3.60 \times 10^{-4}$  Pa calculated from eq. 1 and therefore negligible. For In, the maximum change is ~19 cps/15 min (~4%), or  $\Delta p(In)$  of  $1.25 \times 10^{-5}$  Pa, which is smaller than the error of  $8.20 \times 10^{-5}$  Pa. Hence, even though significant amounts of In are lost over the timescale of hours, variations in Ga and In signals over the duration of single polytherm measurements are negligible.

## 4.4. KEMS - Polytherm

# 4.4.1. Partial pressures of Ga and In

The partial pressures of Ga and In, p(Ga) and p(In), are calculated from the intensities measured above the An-Di glass using eq. 1 within a temperature range of 1550 K to 1740 K (Supplementary Material, Fig. S1, Fig. 2). The ion  $M^+$  is predominant, ions  $MO^+$  and  $M_2^+$  occur at levels near the background, while  $M_2O^+$  is only detected for run 3\_high that has high Ga and In concentrations (7998 and 890-1715 ppm, respectively).

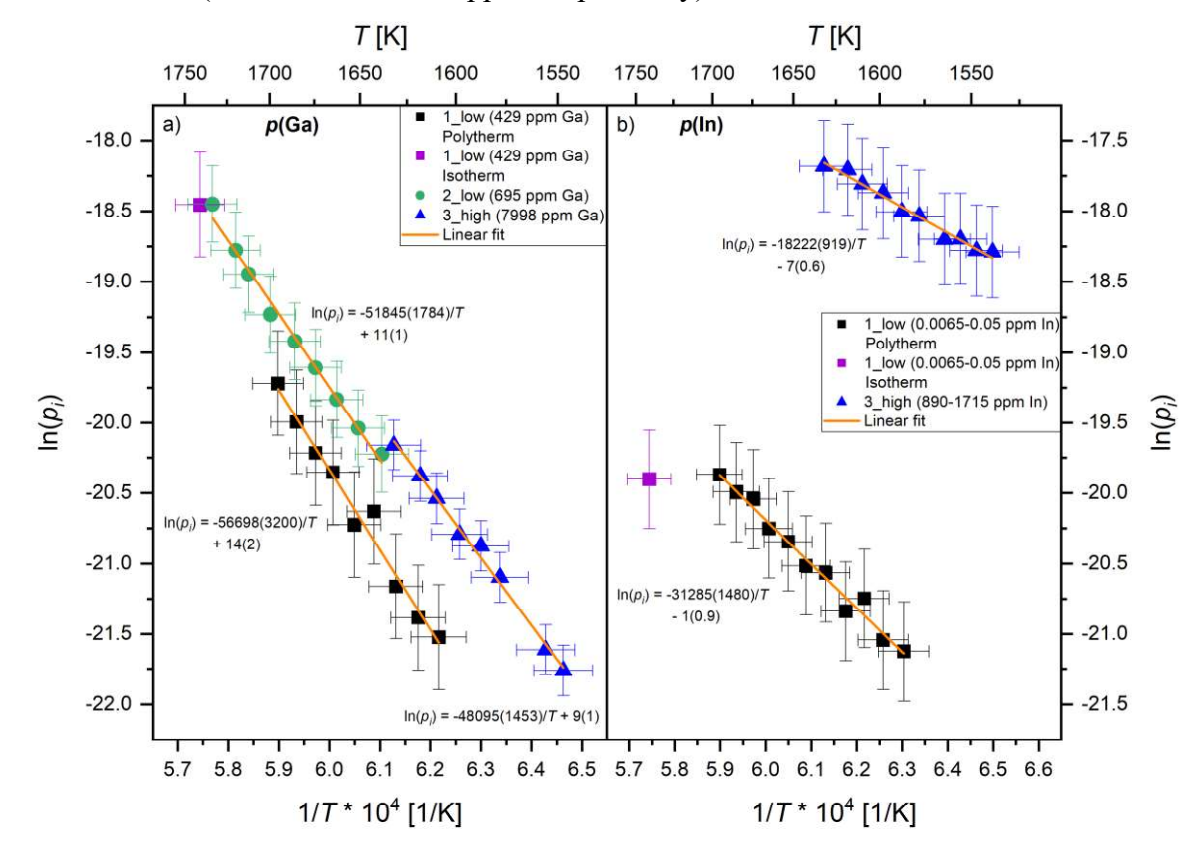


Fig. 2: Partial pressures of a) Ga and b) In above An-Di silicate liquids, determined within a temperature range of 1550 to 1740 K.

For all runs,  $\ln(p_i)$  increases roughly linearly with reciprocal T. Run 2\_low is omitted for In here, since  $\ln(p(\ln))$  in this run only exhibits an increase with reciprocal T to 1500 K, but a decrease afterwards. Thus, for temperatures above the melting point, results of this run are not reliable.

# 4.4.2. Partial pressure of oxygen

The signal of  $O_2$  from the sample (smp; shutter open) is barely resolved from the background (bg, shutter closed);  $[I(O_2^+)_{smp}-I(O_2^+)_{bg}]/I(O_2^+)_{bg}$  is ~0.8 % for 2\_low, whereas it is 20-30 % for 3\_high. Nevertheless, intensity of measured  $O_2^+$  signals do not correlate with those for  $Ga^+$  nor  $In^+$ , as would be expected for the dissociative vaporisation of  $MO_{1.5}$  dissolved in the silicate melt into M or  $M_2O$  gas species (M = Ga or In). Therefore, and given that the evaporation of the W cell container and heating wire also results in  $O_2$  production,  $p_{calc.}(O_2)$  is calculated from stoichiometry (cf. section 3.1). A comparison of  $p_{calc.}(O_2)$  and measured  $p_{meas.}(O_2)$  is given in Fig. 3; for run 1\_low,  $p_{meas.}(O_2)$  was not determined.

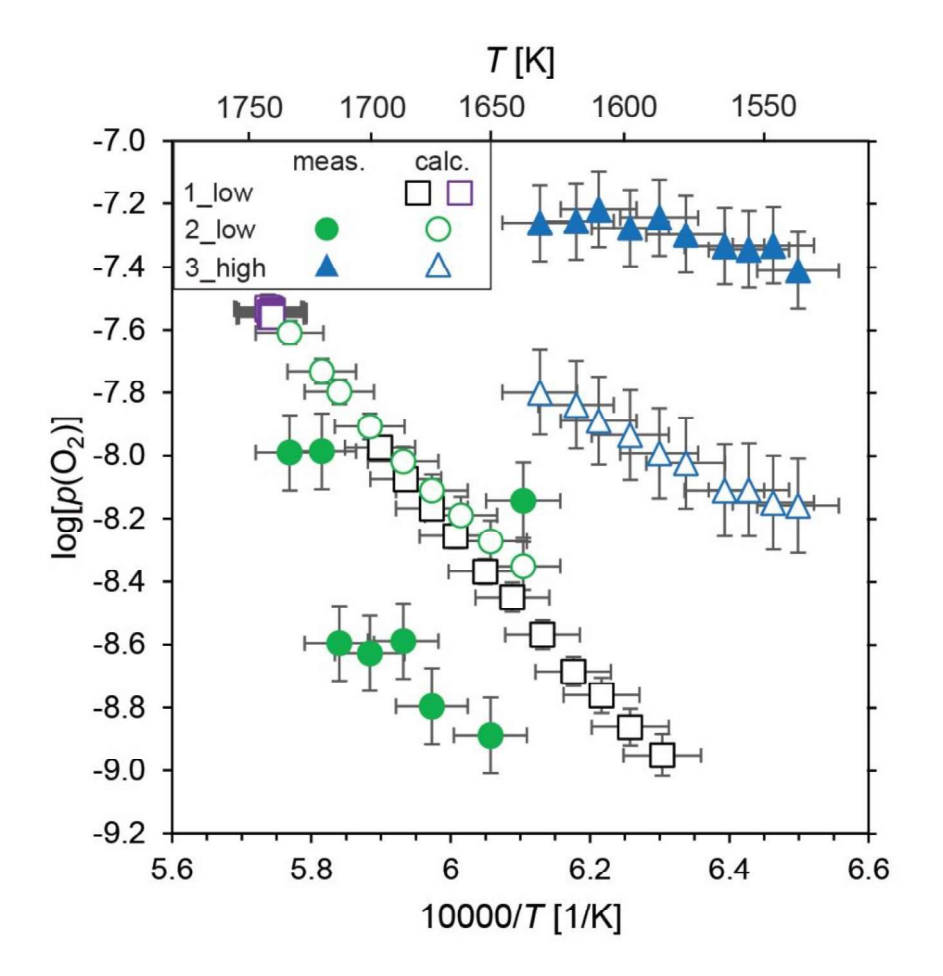


Fig. 3: Comparison of calculated (based on eq. 16; open symbols) and measured (filled symbols) values of  $p(O_2)$ above the An-Di melt in polytherm (1 low - black squares, 2 low - green circles, 3 high - blue triangles) and isotherm (1\_low - purple square) runs.

495 496

497

498

499

500

501

502

503

504

505

506

493

494

The increase of  $log(p_{meas}(O_2))$  in run 2 low is rather scattered, though  $p_{meas}(O_2)$  is only a factor of  $\sim 2$  lower than  $p_{\text{calc.}}(O_2)$ , which, in both run 1 low and run 2 low, increases linearly with reciprocal T. The measured values in 2 low exhibit good agreement ( $\sim$ 3%) with log( $p_{calc.}(O_2)$ ) at 1720 K. As temperature increases, the loss of In, the main contributor to the oxygen partial pressure for run 3\_high, leads to a constant  $p_{\text{meas.}}(O_2)$  within error. The  $p_{\text{calc.}}(O_2)$  for run 3\_high is significantly higher than the 1 low and 2 low runs at the same temperature, which is due to additional O<sub>2</sub> produced by vaporisation of Ga and In-bearing species (cf. eq. 17). For runs 1 low and 2 low,  $p_{\text{calc.}}(O_2)$  is mainly a by-product of MgO and SiO<sub>2</sub> evaporation (~71%), with lesser contributions by Ga (~12%) and In (~17%) at 1630 K. In contrast,  $p_{calc}(O_2)$  for 3 high at 1630 K is dominated by contributions from In ( $\sim$ 70%) and Ga ( $\sim$ 18%) species, and less by Mg + SiO (~12%). For further calculations, only  $p_{\text{calc.}}(O_2)$  is used.

507 508

509 Both 1 low and 2 low runs exhibit a gradual reduction relative to IW (O'Neill and Pownceby, 1993) as temperature increases from 1587 K; ΔIW+1.66 and ΔIW+2.10, respectively, before 510 converging at the highest temperatures ( $\sim$ 1700 K) to a constant value of  $\Delta$ IW+1.54 in both runs. 511 512 Similar, yet slightly elevated  $\Delta IW$  values relative to 1 low and 2 low are observed in run 3 high at a given temperature, owing to the additional contribution of In vaporisation to O<sub>2</sub> in 513 the vapour. It, too, follows a relative decrease as a function of temperature, from  $\Delta IW+2.98$  at 514 1540 K to  $\Delta$ IW+2.33 at 1630 K.

516

517

518

519

520

521

522

515

It should be noted that O also exists as O(g) in high temperature vapours. Provided pressure, temperature and pO<sub>2</sub> are known, its partial pressure can be calculated according to the reaction  $O_2 = 2O$ , which indicates that disproportionation is favoured at higher temperatures (Chase, 1998) and at lower  $pO_2$ . For the highest temperature and  $pO_2$  in our experimental series (isotherm of 1 low at 1740 K), the  $pO_2 = 2.8 \times 10^{-8}$  bar determined (Fig. 3) implies a coexisting pO of  $1.1 \times 10^{-8}$  bar, or roughly a factor  $\sim 3$  lower.

523

4.4.3. Equilibrium constants 524

525

527

526 The partial pressures of Ga and In depend on  $p(O_2)$ , such that the calculation of the activity coefficients of their relevant melt components requires both pO2 and pGa or pIn to be defined above the sample. For this reason, equilibrium constants K are calculated (eq. 22) using  $p_{\text{calc.}}(O_2)$  and compared on a  $\ln(K)$  vs. 1/T plot for the individual runs (Fig. 4).



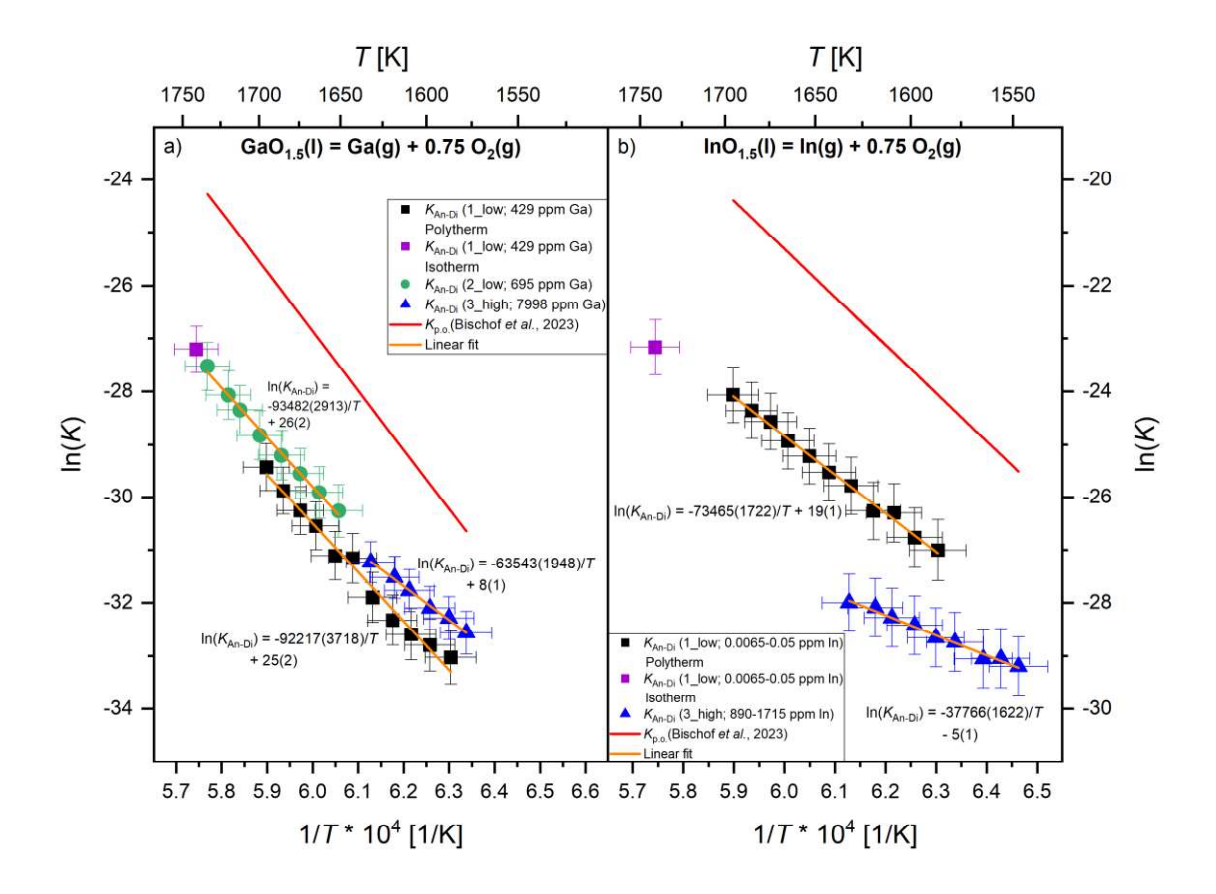


Fig. 4: Equilibrium constants plotted vs. reciprocal temperature (in K) for the reactions, a)  $GaO_{1.5}(l) = Ga(g) + \frac{3}{4}O_2(g)$  and b)  $InO_{1.5}(l) = In(g) + \frac{3}{4}O_2(g)$  as determined above anorthite-diopside eutectic liquid compositions (1\_low, squares – purple = isotherm, black = polytherm; 2\_low, green circles; 3\_high, blue trinagles) as well as for the pure oxides (Bischof et al. 2023) corrected for the latent heat of fusion (red lines; eq. 21).

The calculated equilibrium constants,  $K_{\text{An-Di}}$ , for the Ga vaporisation reaction (Fig. 4a) according to runs 1\_low (polytherm, black and isotherm, purple) and 2\_low are in excellent agreement for both the slope and intercept of the linear fit. For run 3\_high the absolute values of  $K_{\text{An-Di}}$  are in accordance within error with 1\_low and 2\_low, though the slope differs. For the In runs (Fig. 4b), equilibrium constants  $K_{\text{An-Di}}$  determined for the polytherm (black) and isotherm (purple) of run 1\_low are in good agreement. However, there are significant differences between runs 1\_low and 3\_high for the slopes and intercepts of the linear fits with reciprocal temperature. This is likely again due to the high evaporation rate of In over the course of the experiment, see below. The difference between  $K_{\text{p.o.}}$  for the vaporisation reactions above the pure oxides (Bischof *et al.* 2023) and  $K_{\text{An-Di}}$  for the vaporisation reactions above the An-Di melt is the activity coefficient  $\gamma_{i,\text{An-Di}}$  (eq. 23).

# 4.4.4. Activity coefficients

548

549

550

562

563

564

565566

567

568

569

570

571

572

573

574

551 Activity coefficients  $\gamma_i$  for GaO<sub>1.5</sub>(1) and InO<sub>1.5</sub>(1) are calculated as described in section 3.2. using  $\Delta_{\text{fus}}H_{T_{\text{m}}}^{\text{o}}(\text{GaO}_{1.5}) = 49887 \text{ Jmol}^{-1}$  and  $\Delta_{\text{fus}}H_{T_{\text{m}}}^{\text{o}}(\text{InO}_{1.5}) = 52381 \text{ Jmol}^{-1}$  from Lamoreaux 552 et al. (1987), which is in agreement within error with  $\Delta_{\text{fus}}H_{T_{\text{m}}}^{\text{o}}(\text{GaO}_{1.5})=50000~\text{Jmol}^{-1}~\text{from}$ 553 Zinkevich and Aldinger (2004), at the melting points of  $T_m(Ga_2O_3) = 2080 \text{ K}$  and  $T_m(In_2O_3) =$ 554 2186 K (Wood and Wade, 2013). Mole fractions x for the calculation of  $K_{\text{An-Di}}$  (Table 8) are 555 556 derived from LA-ICP-MS measurements (Table 7). For GaO<sub>1.5</sub>, an average of all measurements for each run is taken (Supplementary Material, Fig. S7), whereas for InO<sub>1.5</sub> the mole fractions 557 558 measured near the glass surface are used as this is taken to be in equilibrium with the vapour phase (Supplementary Material, Fig. S8, red points). Since polytherm run 1 low was followed 559 by a 15 h isotherm run leading to a loss of  $GaO_{1.5}$  and  $InO_{1.5}$ , the mole fraction  $x(GaO_{1.5})$  from 560 run 2\_low was used for  $x(GaO_{1.5})$  in polytherm run 1\_low, as both runs are from the same 561

Table 8: Mole fractions  $x_i$  from LA-ICP-MS for the calculation of activity coefficients  $\gamma_i$ . The number in parenthesis gives the uncertainty in the last digit.

starting glass and both polytherms followed the same protocol. For In, for polytherm run 1 low,

 $x(InO_{1.5})$  is corrected by multiplying the LA-ICP-MS-measurements by 1.52, the ratio of the

intensities measured at the beginning (498 cps) and end (326 cps) of the isotherm run (Fig. 1).

Run	Protocol	Concentration	x(GaO <sub>1.5</sub> )	Run	Protocol	Concentration	$x(InO_{1.5})^{\dagger}$
		[ppm]				[ppm]	
1_low	polytherm	429	0.0172(4)*	1_low	polytherm	0.0065-0.05	6.9(7)×10 <sup>-5</sup>
1_low	isotherm	429	0.0136(1)	1_low	isotherm	0.0065-0.05	$5.6(6) \times 10^{-5}$
2_low	polytherm	695	0.0172(4)	2_low	polytherm	-	-
3_high	polytherm	7998	0.0589(3)	3_high	polytherm	890-1715	0.0158(4)

<sup>\*</sup>x from run 2 low also used for run 1 low. See text.

The activity coefficients,  $\gamma_i$ , for both GaO<sub>1.5</sub> and InO<sub>1.5</sub> in the An-Di melt decrease with increasing T, as do the uncertainties, because the contribution of the uncertainty in the  $\Delta_{\text{fus}}G^{\text{o}}$  to the free energy of the vaporisation reaction becomes smaller as temperature approaches  $T_m$  (Fig. 5). These trends cannot be caused by evaporative loss of Ga, which is not observed over the timescales of the polytherm runs. Although  $\gamma(\text{GaO}_{1.5})$  deduced from the stable plateau (Fig.

 $<sup>^{\</sup>dagger}$ Although In concentrations vary with distance to the surface of the melt, only the In concentration at the surface is used to calculate  $x(InO_{1.5})$  in equilibrium with the vapour phase. See text.

5) is within error for all runs and at all temperatures, there are discrete differences (although still within uncertainty) between runs 1\_low and 3\_high for In. For In, the relative decrease in  $\gamma(\text{InO}_{1.5})$  with temperature is of a similar relative magnitude to that of Ga, although evidence for additional loss is visible from the difference in  $\gamma(\text{InO}_{1.5})$  determined by 1\_low Polytherm (black and red points) and 1\_low isotherm (purple point). Consequently, for In in run 1\_low, the most reliable value is that of the isotherm, for which the equilibrium In concentration in the melt was measured. Therefore, the criterion for selecting values of  $\gamma_i$  from the data hinges upon their attainment of a constant value with temperature. Our preferred value is an average of those marked in red in Fig. 5a plus the isotherm value, yielding  $\gamma(\text{GaO}_{1.5}) = 0.036(6)$  at an average T of 1700 K. The value of  $\gamma(\text{InO}_{1.5})$  is within error for all runs (Fig. 5b), too, giving  $\gamma(\text{InO}_{1.5}) = 0.017(12)$  at an average T of 1674 K.

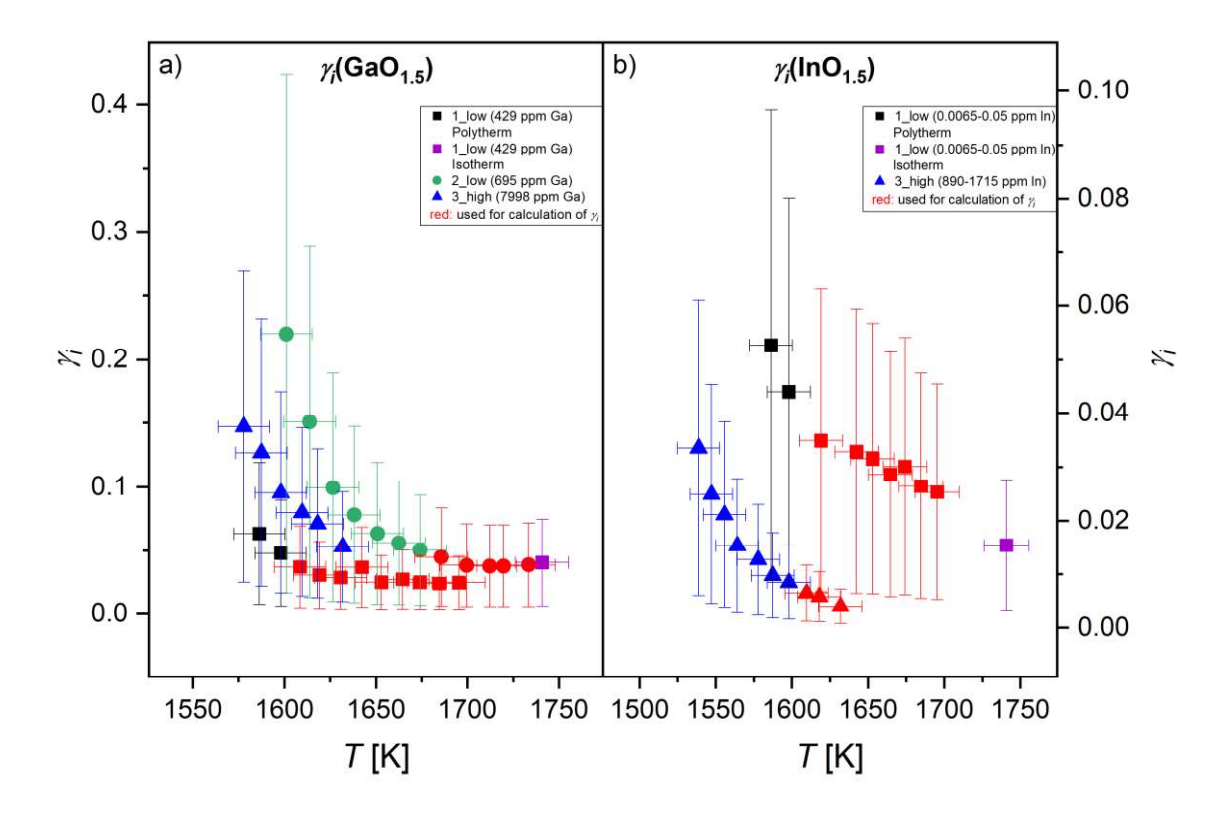


Fig. 5: Temperature dependence of activity coefficients  $\gamma_i$  for a) GaO<sub>1.5</sub> and b) InO<sub>1.5</sub> in anorthite-diopside eutectic melt.

#### 5 Discussion

5.1 Comparison of  $\gamma(InO_{1.5})$  with literature values

As estimates of  $\gamma(\text{GaO}_{1.5})$  in silicate melts are not available in the literature, such a comparison is only feasible for  $\gamma(\text{InO}_{1.5})$ . Ko and Park (2011) and Wood and Wade (2013) both determined

activity coefficients for In species in silicate melts, the former by equilibrating pure In with a silicate melt in the CAS system, whereas the latter exploited its partitioning between CMAS melts and Fe metal together with an expression for  $\gamma$ In in liquid Fe. Ko and Park (2011) conducted their experiments at low oxygen fugacities ( $\Delta$ IW-2.6 to  $\Delta$ IW-1.6) and asserted the stability of InO<sub>0.5</sub>. Given that the oxygen fugacities under which equilibrium was achieved in the melts studied herein ( $\Delta$ IW+1.5 to  $\Delta$ IW+2.5) are at least 3 orders of magnitude higher than in the samples of Ko and Park (2011), we expect that In is present as In<sup>3+</sup> at these fO<sub>2</sub>s. Based on partitioning of In between a Di<sub>28</sub>-Fo<sub>22</sub>-An<sub>50</sub> melt and Fe-rich liquid metal, Wood and Wade (2013) find  $\gamma$ (InO<sub>1.5</sub>) = 0.02 at 1923 K. Their main uncertainty arises from the Margules parameter, W = 52 kJmol<sup>-1</sup>, which is based on a regular solution of Fe-In alloys and a consolute point of 3130 K at Fe<sub>50</sub>In<sub>50</sub>, extrapolated from data to 1700 K (Okamoto, 1990). A conservative error on the value of W of 15% propagates to an uncertainty on  $\gamma$ (In)<sup>∞</sup> of 65% relative and hence a  $\gamma$ (InO<sub>1.5</sub>) of 0.02<sup>+0.015</sup><sub>-0.007</sub>.

The major uncertainty in our value of  $\gamma(\text{InO}_{1.5}) = 0.017(12)$  arises from the concentration profiles of In in the post-KEMS glass. The concentration of In at the surface is that in equilibrium with the p(In) determined at the highest temperatures, with an uncertainty of ~25% relative, *i.e.*  $\gamma(\text{InO}_{1.5})$  of  $0.017^{+0.008}_{-0.005}$ , corresponding to the concentration variations in the boundary region of the glasses. Both temperature (*e.g.* Charles, 1967) and composition (*e.g.* O'Neill and Eggins, 2002) influence the activity coefficients. In terms of temperature, integrating the van't Hoff equation (eq. 24) (Charles, 1967; Sossi et al., 2019)

$$\frac{d\ln(\gamma)}{d(1/T)} = \frac{H}{R'},\tag{24}$$

leads to the activity coefficient approaching unity at infinite temperature. For a regular solution, one can calculate the temperature dependence of the activity coefficient determined at a reference temperature,  $T_1$ , to another temperature,  $T_2$ , by (eq. 25)

$$\ln(\gamma_{T_2}) = \frac{T_1}{T_2} \ln(\gamma_{T_1}), \tag{25}$$

which yields  $\gamma(\text{InO}_{1.5}) = 0.029$  at 1923 K based on our determination at T = 1674 K. This is nominally about 50% higher than that determined by Wood and Wade (2013) but in good agreement considering the uncertainties in both approaches.

Differences may also arise owing to differences in melt composition. To investigate this effect, O'Neill and Eggins (2002) determined  $\gamma(\text{MoO}_2)$ ,  $\gamma(\text{MoO}_3)$ ,  $\gamma(\text{FeO})$ ,  $\gamma(\text{NiO})$  and  $\gamma(\text{CoO})$  in 18 melt compositions in the system CaO-MgO-Al<sub>2</sub>O<sub>3</sub>-SiO<sub>2</sub> at 1673 K under controlled oxygen fugacity in equilibrium with the pure metal. They found the melt oxide species of divalent metal cations,  $\gamma(\text{FeO})$ ,  $\gamma(\text{NiO})$  and  $\gamma(\text{CoO})$  to vary within a factor two over the investigated compositional range, but without specific major oxide dependencies. In contrast, activity coefficients of the melt oxide components of more highly charged cations, MoO<sub>2</sub> and MoO<sub>3</sub>,

vary by factors of 20 and 60 and correlate with CaO in the melt, "suggesting the influence of

CaMoO<sub>3</sub> and CaMoO<sub>4</sub> complexes" (O'Neill and Eggins, 2002). Trivalent In in our silicate

glasses may be expected to behave in a manner intermediate to that of the  $M^{2+}$  and  $M^{4+}/M^{6+}$ 

cations studied by O'Neill and Eggins (2002).

Typically, the magnitudes of the activity coefficients of oxide species in silicate melts are rationalised by comparison with the free energies of solid compounds with similar stoichiometries (*e.g.* O'Neill and Eggins, 2002). Given the existence of gallium analogues of albite (NaGaSi<sub>3</sub>O<sub>8</sub>) and anorthite (CaAlGaSi<sub>2</sub>O<sub>8</sub>) (Goldsmith, 1950; Fegley *et al.*, 2023), an influence of melt composition on the activity coefficients of GaO<sub>1.5</sub> (and InO<sub>1.5</sub>) cannot be excluded. Namely,  $\gamma$ (MO<sub>1.5</sub>) may decrease as silica, alumina and lime activities in the melt increase owing to a reaction of the type (eq. 26):

$$A^{1+n}O_{\frac{1+n}{4}} + nAlO_{1.5} + MO_{1.5} + (3-n)SiO_2 = A^{1+n}MAl_nSi_{(3-n)}O_8$$
 (26)

where A = an alkali (n = 0) or alkaline earth (n = 1) metal, and M = Ga or In. Additional experiments would shed light on the dependence of  $\gamma(MO_{1.5})$  on liquid composition.

Finally, the calculation of  $\gamma(\text{InO}_{1.5})$  in Wood and Wade (2013) is based on the assumption of an entropy of fusion  $\Delta_{\text{fus}}S^{\text{o}}_{T_{\text{m}}}$  of 26.25 JK<sup>-1</sup> for InO<sub>1.5</sub> at a melting point of 2183 K, a value close to that for GaO<sub>1.5</sub>, 26.3 JK<sup>-1</sup>. Lamoreaux *et al.* (1987) report  $\Delta_{\text{fus}}H/R$  values of 12.0 ± 2.4 kK for Ga<sub>2</sub>O<sub>3</sub> at 2080 K and 12.6 ± 1.2 kK for In<sub>2</sub>O<sub>3</sub> at 2186 K, which are estimated values with significant uncertainties, based on Glushko *et al.* (1981), Pankratz (1982) and Wagman *et al.* (1982). These values correspond to  $\Delta_{\text{fus}}S^{\text{o}}_{T_{\text{m}}}(\text{GaO}_{1.5}) = 23.98$  JK<sup>-1</sup> and  $\Delta_{\text{fus}}S^{\text{o}}_{T_{\text{m}}}(\text{InO}_{1.5}) = 23.96$  JK<sup>-1</sup>, substantiating the assumption that entropies of fusion for Ga and In sesquioxides are similar. The uncertainties reported on  $\Delta_{\text{fus}}H/R$  correspond to a difference of ±10 – 15 %

relative, depending on temperature, and are included in the uncertainty on  $\gamma GaO_{1.5}$  and  $\gamma InO_{1.5}$ .

Use of the values of Wood and Wade (2013) for the entropy of fusion would result in a  $\sim$ 10 %

relative increase in the  $\gamma GaO_{1.5}$  and  $\gamma InO_{1.5}$  values reported here.

662663

661

5.2 Silicate melt activity coefficients for oxides of group 13 elements

664

665 Elements of the same group often share structural similarities within silicate melts (e.g.

Ryerson, 1985). Indeed, a general decrease in the activity coefficients of alkali oxides in binary

A<sub>2</sub>O-SiO<sub>2</sub> silicate melts down the group is observed (Charles, 1967), with decreasing Z/r (Z =

charge, r = ionic radius). The group 6 oxides of Cr, Mo and W exhibit similar behaviour:

Pretorius and Muan (1992) determine  $\gamma(CrO_{1.5}) = 24.7$  in CaO-Al<sub>2</sub>O<sub>3</sub>-Cr<sub>2</sub>O<sub>3</sub>-SiO<sub>2</sub> melts at  $\Delta$ IW-

3 and 1773 K. At the same temperature, for a An-Di eutectic composition, O'Neill and Eggins

671 (2002) obtained  $\gamma(MoO_3) = 0.303$  and O'Neill *et al.* (2008) found  $\gamma(WO_3) = 0.07$ . Although the

group 6 metals increase in valence down the group ( $Cr^{3+}$  to  $Mo^{4+/6+}$  and  $W^{4+/6+}$ ; Mallmann et

al., 2021), their corresponding melt oxide activity coefficients decrease.

(Wu and Stebbins, 2010), while data for In are lacking.

674

675

676

677

678679

680

681

682

683

684

685

686

687

688

689

690

673

670

Fegley et al. (2023) suggested that the activity coefficients of the Group 13 elements from Al to In would show progressively larger negative deviations from ideality, based on their optical basicity and Z/r, as well as scarce experimental data for Al and In. Central to testing this hypothesis is the comparison of the new results for  $\gamma(\text{GaO}_{1.5})$  and  $\gamma(\text{InO}_{1.5})$  presented herein with literature data for the group 13 elements B and Al (Fig. 6). Boike *et al.* (1993) investigated thermodynamic activities in B<sub>2</sub>O<sub>3</sub>-SiO<sub>2</sub> melts with 20 and 90 mol% B<sub>2</sub>O<sub>3</sub> using KEMS, and found  $\gamma(\text{BO}_{1.5}) = 0.96$  at 1475, although these compositions were not in the Henry's law region as in this work. The Slag-Liq model of FactSage, for a B content of 10 ppm (inferred to be at infinite dilution) yields  $\gamma(\text{BO}_{1.5}) = 8 \times 10^{-4}$ , similar to the  $4 \times 10^{-4}$  for Fe-bearing systems calculated by the same solution model (Fegley *et al.* 2023). The activity coefficient  $\gamma(\text{AlO}_{1.5})$  of 0.39 at 1674 K for an anorthite-diopside melt composition is calculated from VapoRock (Wolf et al., 2023), which is based on the MELTS liquid model (Ghiorso and Sack, 1995) and gas species properties from thermochemistry tables such as NIST-JANAF (Chase, 1998). In Fig. 6, all elements are assumed to exist in IV-fold coordination in the glass, which is a sound assertion for Al and Ga (*cf.* Mare *et al.*, 2021), whereas B may in part have 3-fold coordination

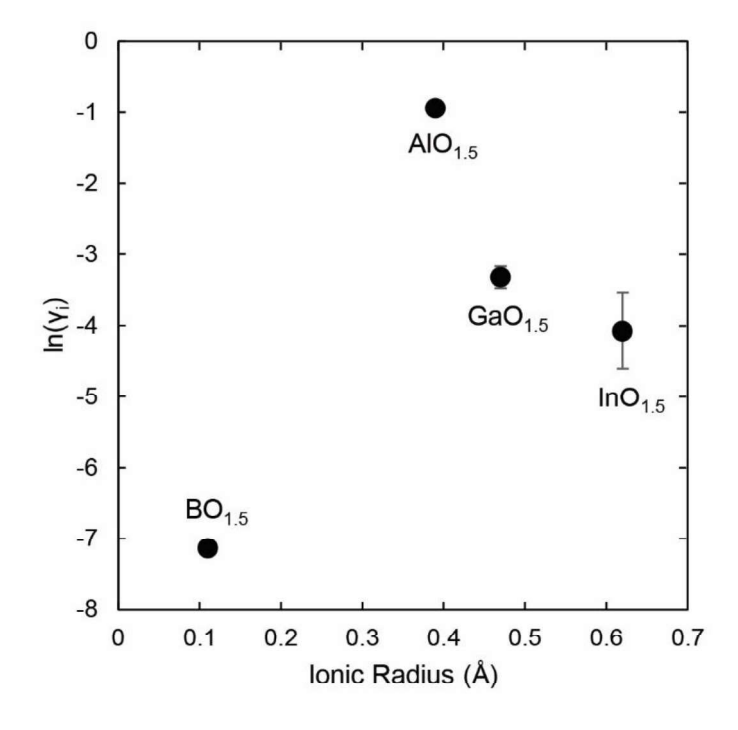


Fig. 6: Comparison of activity coefficients of group 13 metal oxides at 1674 K in anorthite-diopside eutectic melts. All metals are assumed to be IV-fold coordinated with oxygen, with their corresponding ionic radii from Shannon (1976).

#### 5.3 Comparison with volatilities of K and Zn

The observed depletions of volatile elements in the bulk silicate Earth (BSE) relative to CI chondrites are testimony to the nature of the processes that led to the accretion of the Earth (e.g., Mezger et al. 2021; Sossi et al. 2022; Solomatova & Caracas, 2023). Lithophile volatile elements, in particular, are useful in that they ought not to be present to any significant extent in the Earth's core. Gallium and indium, however, have been shown experimentally to partition into core-forming Fe-Ni alloy to appreciable amounts ( $D_{\text{met-sil.}} \sim 5 - 30$ ; Mann et al. 2009; Blanchard et al. 2015; Wang et al. 2016) and, as such, should be depleted in the BSE relative to lithophile elements of similar volatility. This expectation notwithstanding, the BSE abundances of Ga and In are similar to, or higher than, respectively, those of lithophile elements with comparable  $T_c^{50}$  (e.g., Wood et al. 2019). One potential explanation states that  $T_c^{50}$  is not an appropriate descriptor of element volatility during their evaporation from silicate melts, a process that may have played a role in volatile depletion in the building blocks of the Earth (e.g., Hin et al. 2017).

In order to quantify the magnitude of the relative difference in volatility under nebular and planetary conditions, we compare the partial pressures of Ga with K and of In with Zn, given

that these two element pairs have similar CI- and Al-normalised abundances in the BSE, as well as comparable  $T_c^{50}$ . To do so, we use our activity coefficients for GaO<sub>1.5</sub> and InO<sub>1.5</sub> together with literature data for ZnO and KO<sub>0.5</sub> (Sossi et al., 2019), and calculate partial pressures for Ga, K, In and Zn as a function of temperature and  $fO_2$  at a total pressure of 1 bar (Supplementary Material; Fig. 7). The white line marks the conditions at which partial pressures are equivalent.

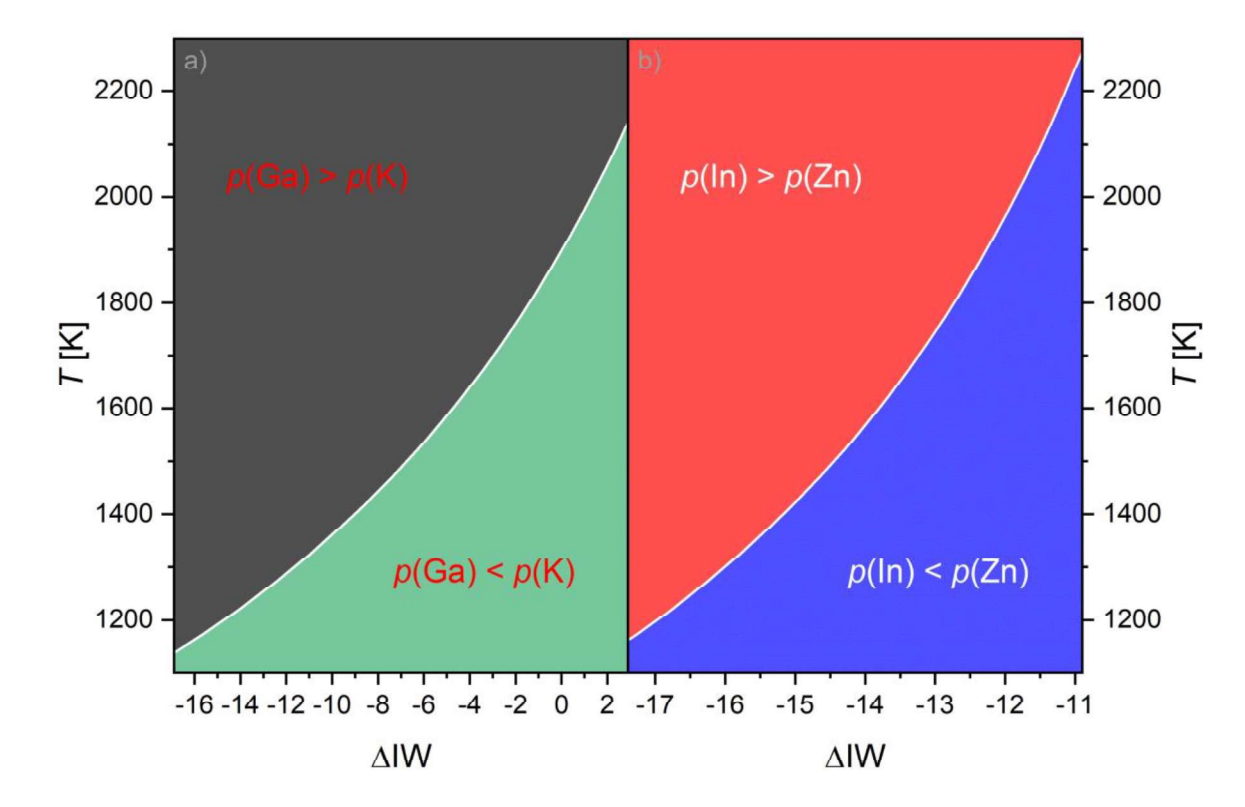


Fig. 7: Partial pressures of a) Ga vs. K and b) Zn vs. In, in a plot of  $\Delta IW vs$ . temperature at 1 bar. Evaporation of silicate melts is expected to occur >1600 K and between IW-2 to IW+3 (e.g., Visscher and Fegley, 2013).

For regions in which basaltic melts are stable, at  $\sim$ 1600 K and above, potassium is found to be more volatile than gallium, provided the  $fO_2$  remains at IW-4 or above. At constant temperature, increasing  $fO_2$  favours the vaporisation of K over Ga, which can be rationalised by their respective vaporisation stoichiometries. For generalised equilibria of the form

$$M^{x+n}O_{\frac{x+n}{2}}(l) = M^xO_{\frac{x}{2}}(g) + \frac{n}{4}O_2(g), (27)$$

gallium oxide has a vaporisation reaction in which n = 3 (this work, Sossi *et al.* 2019) whereas that for K, as an alkali metal that occurs as a monovalent cation in silicate melts, defines an n = 1 reaction. Hence, the ratio of their partial pressures, p(Ga)/p(K), is proportional to  $f(O_2)^{-0.5}$ . As a result, K is expected to be more volatile than Ga during evaporation from silicate liquids,

except under reducing conditions ( $\Delta IW < 0$ ) at very high temperatures (>2000 K). The picture is clearer for zinc, which is more volatile than In under all relevant conditions ( $\Delta IW > -4$ ). This outcome mirrors the conclusions of Liu *et al.* (2022), who find Zn to be more volatile than In above basaltic melts between 1573 – 1773 K and log( $fO_2$ ) from  $\Delta IW + 10$  to  $\Delta IW = 0$ . The dependence on  $fO_2$  is weaker than for Ga and K, because p(In)/p(Zn) is proportional to  $f(O_2)^{-0.25}$ , as In and Zn define n = 3 and n = 2 reactions, respectively (Sossi *et al.* 2019; Liu *et al.* 2022; this work).

5.4 Condensation temperatures of Ga, In, Zn and K from anorthite-diopside eutectic melts

A common way of quantifying the volatility of an element is through the calculation of its 50 % condensation temperature. While this exercise is typically performed for a system whose bulk composition is that of the solar nebula (e.g. Lodders, 2003), Fegley et al. (2023) recently calculated the condensation sequence for 69 elements for a BSE composition. The temperature at which 50 % of the mass of an element, i, condenses,  $T_c^{50}$ , can be found by equating the following expressions for the partial pressure of its stable gas species (in the limit of a single dominant gas species for a given element):

$$p_i = \alpha_i \frac{N_i}{N_T} P_T, (28)$$

752 with

753 
$$p_i = \frac{K_{(27)}a\left(M^{x+n}O_{\underline{x+n}}\right)}{f(O_2)^{\frac{n}{4}}}(29)$$

where  $a_i$  is the mass fraction of i in the gas phase (here set to 0.5),  $N_i$  and  $N_T$  are the abundances of element i and of the sum of all elements in the gas phase, respectively, and  $P_T$  is the total pressure (see Larimer, 1967). For the solar nebula,  $N_T$ , to a very good approximation, is equivalent to the sum of  $N(H_2)$  and  $N(H_2)$ , while  $N_T$  remains essentially constant throughout the temperature range over which equilibrium is computed because neither  $H_2$  nor  $H_2$  and  $H_3$  consequently,  $N_T$  decreases significantly as condensation of major elements (Al, Ca, O, etc.) progresses down-temperature at constant  $P_T$ . To properly account for changes in  $N_T$ , we use FactSage 8.2 (Bale et al., 2016) to calculate the 50 % condensation temperatures of  $G_3$ ,  $G_4$ ,  $G_4$ ,  $G_5$ ,  $G_7$ ,

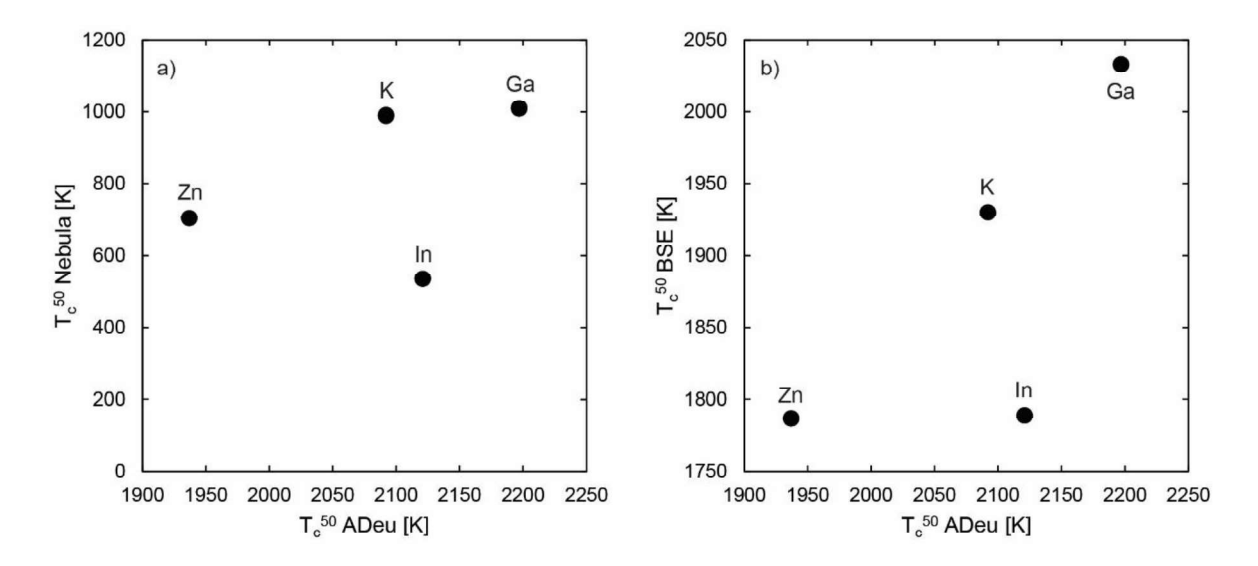


Fig. 8: Comparison of volatilities of Ga, K, In and Zn calculated based on their 50 % condensation temperatures from an anorthite-diopside eutectic melt ( $T_{c,ADeu}^{50}$ ) at  $10^{-4}$  bar (this work) and **a)** their nebular  $T_c^{50}$  (Wood et al., 2019) **b)** their  $T_{c,BSE}^{50}$  (Fegley *et al.* 2023).

Table 9: 50 % condensation temperatures of Ga, In, K and Zn above a silicate liquid of anorthite-diopside eutectic composition using the Slag-LiqA model of FactSage 8.2. (Bale *et al.* 2016), with Henrian activity coefficients for  $Ga_2O_3(l)$  and  $In_2O_3(s)$  of the form  $log_{10}(\gamma_i) = A/T + B$ , based on this work. For  $Ga_2O_3(l)$ , A = -4800, B = 0 and for  $In_2O_3(s)$ , A = -7230 and B = 0.

-	$P_T = 10^{-6} \text{ bar}$		$P_T =$	10 <sup>-4</sup> bar	$P_T = 10^{-2} \text{ bar}$	
	$\Delta IW$ at $T_c{}^{50}$	Tc <sup>50</sup> ADeu [K]	$\Delta IW$ at $T_c{}^{50}$	T <sub>c</sub> <sup>50</sup> ADeu [K]	$\Delta IW$ at $T_c{}^{50}$	T <sub>c</sub> <sup>50</sup> ADeu [K]
Ga	1.33	1874	1.20	2197	1.08	2662
In	1.99	1781	1.55	2121	1.26	2611
K	2.43	1733	1.74	2092	1.26	2610
Zn	4.31	1568	2.96	1937	1.66	2515

In comparison to nebular  $T_c^{50}$  (Fig. 8a), condensation temperatures from silicate melts are higher at the same  $P_T$ , owing to the fact that the  $fO_2$  (relative to IW) is much lower in the former case ( $\sim$ ΔIW-7), which increases  $p_i$  for the four elements considered (eq. 29). This effect is most pronounced for Ga(g) and In(g), whose partial pressures depend on  $fO_2^{-3/4}$  (compared to an exponent of -1/2 for Zn and -1/4 for K). Moreover, additional gas species, such as InCl (Wai and Wasson, 1977) allow In to remain in the vapour to lower temperatures in the solar nebula. For silicate melts, Ga is clearly more refractory than K and the calculations of Fegley *et al.* (2023) show that Zn and In have similar  $T_{c,BSE}^{50}$ , whereas In condenses at temperatures similar to K (and higher than Zn) above anorthite-diopside eutectic melts (Fig. 8b). Evaporation experiments (Liu et al., 2022; Norris and Wood, 2017) indicate that Zn is more volatile than In at the IW buffer, the  $fO_2$  near which In and Zn condense in anorthite-diopside eutectic liquids (Table 9). The linear temperature offset between  $T_{c,ADeu}^{50}$  and  $T_{c,BSE}^{50}$  likely comes from the absence of a large number of gaseous species (namely Fe) in the anorthite-diopside system

relative to the BSE, thereby increasing  $N_i/N_T$  (eq. 28) at constant  $P_T$  and hence increasing  $T_{c,ADeu}^{50}$  relative to  $T_{c,BSE}^{50}$ . Evaporative loss of these elements from a silicate melt is able, qualitatively, to account for the apparent overabundance of Ga and In in BSE compared to elements initially thought to be more refractory, such as K and Zn. That is, volatility based on evaporation of a silicate melt is in the order (from least to most volatile) Ga < K ~ In < Zn, consistent with their relative abundances in the BSE.

# 5.5 Application to chondrules

Chondrules, mm- to cm-sized spherules of silicate-rich composition, are near-ubiquitous components of eponymous chondrites, and have also been mooted to contribute significantly to the accretion of the terrestrial planets (Alexander, 2019). As such, the modes of their genesis are potentially significant in understanding volatile depletion processes in the early Solar System. The formation of chondrules is thought to progress by rapid heating of primitive condensates in the solar nebula gas reaching temperatures sufficient to cause melting (> 1500 K, e.g., Grossman and Wasson, 1982; Connelly et al., 2012). This process took place over sufficiently long timescales that chemical equilibrium between the gas and the chondruleforming liquid was reached, a conclusion based on the lack of stable isotope fractionation of moderately volatile elements in the chondrules, namely K (Alexander et al., 2000; Richter et al., 2011; Yu et al., 2003). Consequently, it remains unclear as to whether chondrules, depleted in moderately volatiles with respect to the matrix components of chondrites (Bland et al., 2005; Grossman and Wasson, 1985), acquired their composition during their formation, or whether volatile depletion was inherited from their precursors, the earliest solid condensates (Alexander et al., 2008). To examine whether such depletions could have been caused by evaporation, we model the elemental composition of evaporation residues using trace elements whose evaporation behaviour is well-defined (Ga, Ge, In, Pb, Ag, Zn, Rb; this work; Sossi et al., 2019).

The matrix mass fraction of different carbonaceous chondrite (CC) types correlates linearly with the abundance of a given moderately volatile element and passes through the CI abundance (Alexander, 2019; Hellmann et al., 2020). Owing to the fact that a CI-like matrix component is common to all CCs, the intercept at zero matrix fraction yields the 'non-matrix' or chondrule component present in the CCs. The mean chondrule composition derived in such a manner (after Hellmann *et al.* 2020) is used as the target value for our calculations, in which temperature and  $fO_2$  are varied in an attempt to reproduce the observed depletion from CI-like precursor

material, following the approach of Sossi *et al.* (2019) and Tartèse *et al.* (2021). This involves fixing fZn, the fraction of Zn that has evaporated, to 0.12 (the observed value) and calculating the relative depletion factors of the other elements.

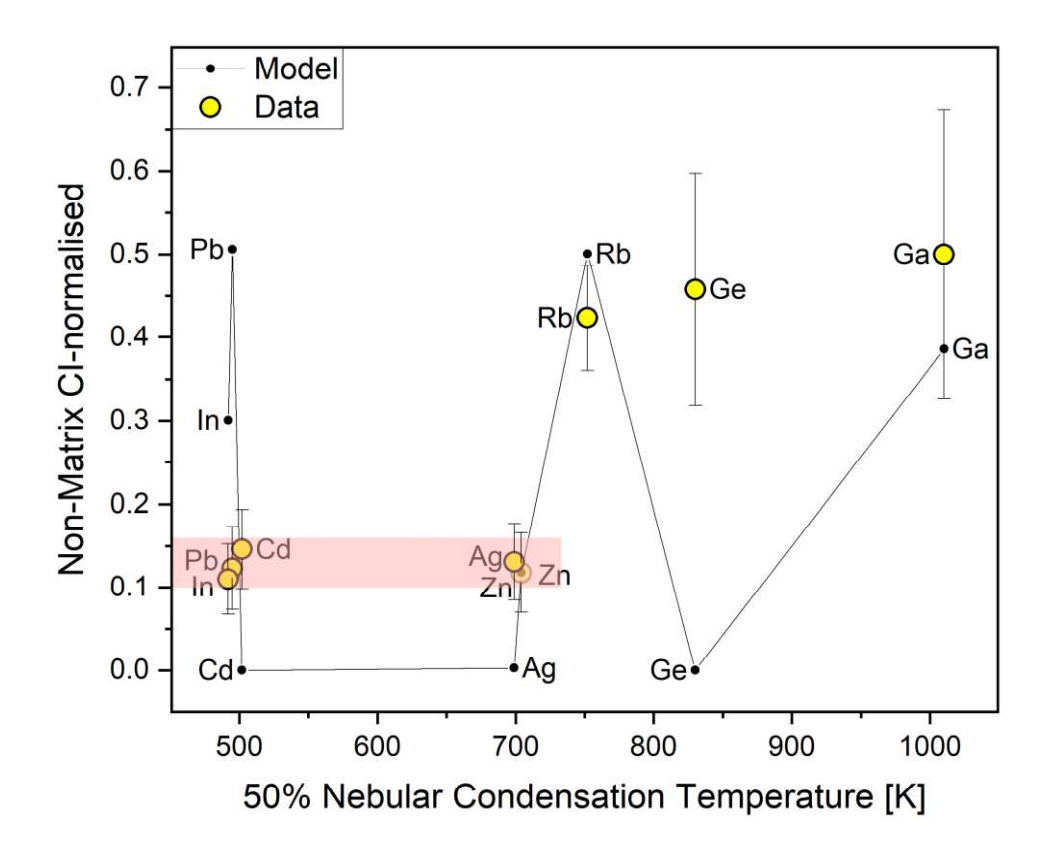


Fig. 9: Elemental composition normalised to CI chondrites of the 'non-matrix' component, taken to represent the average chondrule composition, in carbonaceous chondrites. Yellow points represent the data as calculated by Hellmann *et al.* (2020) and the black lines represent the best-fit model calculated at 2650 K and  $\Delta$ IW+1.4. The red bar indicates a constant abundance plateau of  $0.13 \pm 0.03 \times CI$ .

Minimisation of the objective function returns a temperature of 2650 K and  $\Delta IW+1.4$  for which adequate fits, within uncertainty, are obtained for Ga and Rb, while Pb and In are within a factor of 3. Notwithstanding a resulting  $fO_2$  too high to account for the presence of metal observed in many chondrules, Cd, Ag and Ge in the chondrules are far too abundant than can be accounted for by evaporation. While evaporation from silicate melts is considered here only in the anhydrous limit (*i.e.*, equilibria of the form of eq. 27), thermodynamic data for metal hydrides and -hydroxides (MH and MOH, where M = In, Pb, Ge, Ga, Cd, or Zn) indicate that these species only become significant at nebular  $pH_2O/pH_2$  ratios ( $5\times10^{-4}$ ) at pressures > 10 bar at 2000 K. As such, this reaction stoichiometry is likely to be appropriate for moderately volatile elements under the modest total pressures ( $\leq 1$  bar) of the solar nebula.

Rather, the most plausible explanation is that the chemistry of the non-matrix component is inherited from the chondrule precursor material, and that chondrules did not undergo significant evaporation and loss of moderately volatile elements during their formation (Rubin, 2000). It appears instead that chondrule precursors themselves experienced volatile depletion before being overprinted by a CI-like component. This pattern is similar to that found in bulk chondrites themselves (*e.g.*, Braukmüller *et al.* 2018), which may indicate that chondrule precursors were formed in a manner similar to those of chondrites. Such an explanation would be consistent with the lack of stable isotope fractionation observed in chondrules, together with the correlation of volatile- with non-volatile incompatible elements (*e.g.*, Na with rare-earth elements, REE, Grossman and Wasson, 1985) in some chondrules. Because even the most volatile elements, Cd and Ag, are present in CI-chondritic proportions, the confining pressures during melting of chondrule precursors must have been significant in order to prevent their evaporative loss.

# **6 Conclusion**

Knudsen Effusion Mass Spectrometry (KEMS) allowed us to precisely determine the prevailing gas species (Ga<sup>0</sup> and In<sup>0</sup>) and activity coefficients of GaO<sub>1.5</sub> and InO<sub>1.5</sub> in an anorthite-diopside eutectic silicate melt (at relatively oxidising conditions; ΔIW+1.5 to +2.5) to 0.036(6) and 0.017(12), respectively. Combining these determinations with those for other group 13 elements, we find a trend of decreasing activity coefficients down the group that is inversely correlated with ionic radius, with B being an exception. Having defined their evaporation reactions from silicate melts, the partial pressures of Ga, K, In and Zn as a function of temperature and fO2 show that their relative volatilities above An-Di eutectic liquid differ considerably from those given by their 50% condensation temperatures  $T_c^{50}$  for solar nebular conditions. The relative order of volatility from silicate melts (from least to most volatile) is Ga < K ~ In < Zn, broadly matching their relative abundances in the BSE. As a result, the hypothesis that the abundances of moderately volatile elements in BSE, such as Ga and In, were not set under nebular, but rather under oxidising conditions by depletion from silicate liquids at later stages of planetary accretion, appears plausible and warrants further investigation. Based on the volatilities of Ga and In compared to other moderately volatile elements, we show that chondrules likely did not undergo evaporative loss during melting.

Acknowledgements

LB and PAS were supported by a Swiss National Science Foundation (SNSF) Ambizione Fellowship (#180025). LB thanks Julien Allaz and Pete Tollan for assistance on the electron microprobe and laser-ablation mass spectrometer, respectively. We thank Ralf Küppers for support at FZJ. We are grateful to Bruce Fegley, Nate Jacobson and Remco Hin for perceptive comments in their comprehensive reviews of our work, and to Bernard Charlier for the editorial handling of our article.

Appendix A. Supplementary Material

The data of the partial pressures, equilibrium constants, and activity coefficients for KEMS runs are provided, as well as the abundances of major and trace elements in glasses, pre- and post-experiment as determined by EPMA and by LA-ICP-MS, respectively, are reported.

## 885 References

- Alexander, C.M.O., Grossman, J.N., Wang, J., Zanda, B., Bourot-Denise, M., Hewins, R.H.,
- 888 2000. The lack of potassium-isotopic fractionation in Bishunpur chondrules. Meteorit.
- 889 Planet. Sci. 35, 859–868.
- Alexander, C.M.O.D., 2019. Quantitative models for the elemental and isotopic fractionations
- in chondrites: The carbonaceous chondrites. Geochim. Cosmochim. Acta 254, 277–309.
- 892 https://doi.org/10.1016/j.gca.2019.02.008
- Alexander, C.M.O.D., Grossman, J.N., Ebel, D.S., Ciesla, F.J., 2008. The formation
- conditions of chondrules and chondrites. Science (80-.). 320, 1617–1619.
- Armstrong, J.T., 1988. Quantitative analysis of silicates and oxide minerals: Comparison of
- Monte-Carlo, ZAF and Phi-Rho-Z procedures. Microbeam Anal. 239–246.
- Bale, C.W., Bélisle, E., Chartrand, P., Decterov, S.A., Eriksson, G., Gheribi, A.E., Hack, K.,
- Jung, I.H., Kang, Y.B., Melançon, J., Pelton, A.D., Petersen, S., Robelin, C., Sangster, J.,
- van Ende, M.-A., 2016. FactSage Thermochemical Software and Databases, 2010-2016.
- 900 Calphad 54, 35 53.
- 901 Bischof, L., Sossi, P.A., Sergeev, D., Müller, M., Schmidt, M.W., 2023. Quantification of
- thermodynamic properties for vaporisation reactions above solid Ga2O3 and In2O3 by
- 903 Knudsen Effusion Mass Spectrometry. Calphad 80, 102507.
- 904 https://doi.org/10.1016/j.calphad.2022.102507
- 905 Bland, P.A., Alard, O., Benedix, G.K., Kearsley, A.T., Menzies, O.N., Watt, L.E., Rogers,
- N.W., 2005. Volatile fractionation in the early solar system and chondrule/matrix
- 907 complementarity. Proc. Natl. Acad. Sci. U. S. A. 102, 13755–13760.
- 908 Boike, M., Hilpert, K., Müller, F., 1993. Thermodynamic Activities in B2O3 SiO2 Melts at
- 909 1475 K. J. Am. Ceram. Soc. 76, 2809–2812.
- 910 Charles, R.J., 1967. Activities in Li2O-, Na2O-, and K2O-SiO2 Solutions. J. Am. Ceram.
- 911 Soc. 50, 631–641.
- Chase, M.W., 1998. NIST-JANAF Thermochemical Tables. 4th Ed. J. Phys. Chem. Ref. Data
- 913 Monogr. 9, Parts I II.
- Connelly, J.N., Bizzarro, M., Krot, A.N., Nordlund, Å., Wielandt, D., Ivanova, M.A., 2012.
- The absolute chronology and thermal processing of solids in the solar protoplanetary
- 916 disk. Science (80-. ). 338, 651–655.
- 917 Copland, E.H., Jacobson, N.S., 2010. Measuring Thermodynamic Properties of Metals and
- 918 Alloys With Knudsen Effusion Mass Spectrometry.

- 919 https://doi.org/10.1002/9781118180730.ch48
- 920 Costa, G.C.C., Jacobson, N.S., Fegley, B., 2017. Vaporization and thermodynamics of
- 921 forsterite-rich olivine and some implications for silicate atmospheres of hot rocky
- 922 exoplanets. Icarus 289, 42–55. https://doi.org/10.1016/j.icarus.2017.02.006
- Donovan, J.J., Singer, J.W., Armstrong, J.T., 2016. A new EPMA method for fast trace
- element analysis in simple matrices. Am. Mineral. 101, 1839–1853.
- 925 https://doi.org/10.2138/am-2016-5628
- 926 Donovan, J.J., Tingle, T.N., 1996. An Improved Mean Atomic Number Background
- 927 Correction for Quantitative Microanalysis. J. Microsc. 2, 1–7.
- Drowart, J., Chatillon, C., Hastie, J., Bonnell, D., 2005. High-temperature mass spectrometry:
- Instrumental techniques, ionization cross-sections, pressure measurements, and
- thermodynamic data (IUPAC Technical Report). Pure Appl. Chem. 77, 683–737.
- 931 https://doi.org/10.1351/pac200577040683
- Drowart, J., Goldfinger, P., 1967. Investigation of Inorganic Systems at High Temperature by
- 933 Mass Spectrometry. Angew. Chemie Int. Ed. English 6, 581–596.
- 934 https://doi.org/10.1002/anie.196705811
- Ebel, D.S., 2004. Condensation of rocky material in astrophysical environments, in: Lauretta,
- D.S., McSween, H.Y.J. (Eds.), Meteorites and the Early Solar System II. University of
- 937 Arizona Press, Tucson, pp. 253–277.
- Elkins-Tanton, L.T., 2012. Magma oceans in the inner solar system. Annu. Rev. Earth Planet.
- 939 Sci. 40, 113–139. https://doi.org/10.1146/annurev-earth-042711-105503
- 940 Fegley, B., Lodders, K., Jacobson, N.S., 2023. Chemical Equilibrium Calculations for Bulk
- 941 SIlicate Earth Material at High Temperatures. Geochemistry 82, 125961.
- 942 Fite, W.L., Brackmann, R.T., 1959. Ionization of Atomic Oxygen on Electron Impact. Phys.
- 943 Rev. 113, 815–816. https://doi.org/10.1103/PhysRev.113.815
- 944 Ghiorso, M.S., Sack, R.O., 1995. Chemical mass transfer in magmatic processes IV. A
- revised and internally consistent thermodynamic model for the interpolation and
- extrapolation of liquid-solid equilibria in magmatic systems at elevated temperatures and
- pressures. Contrib. to Mineral. Petrol. 119, 197–212.
- 948 https://doi.org/10.1007/BF00307281
- Glushko, V.P., Gurvich, L. V., Bergman, G.A., Veitz, I. V., Medvedev, V.A., Khachkuruzov,
- 950 G.A., Yungman, V.S., 1981. Thermodynamic Data for Individual Substances, Vol. 3:
- The elements B, Al, Ga, In, Tl, Be, Mg, Ca, Sr, and Ba and their compounds. Nauka,
- 952 Moscow.

- 953 Goldsmith, J.R., 1950. Gallium and Germanium Substitutions in Synthetic Feldspars. J. Geol.
- 954 58.
- 955 Gomez, M., Chatillon, C., Allibert, M., 1982. Thermodynamics of gaseous and condensed
- indium oxides by mass spectrometry with controlled oxygen pressure. J. Chem.
- 957 Thermodyn. 14, 447–459. https://doi.org/10.1016/0021-9614(82)90137-9
- 958 Grossman, J.N., Wasson, J.T., 1985. The origin and history of the metal and sulfide
- components of chondrules. Geochim. Cosmochim. Acta 49, 925–939.
- 960 https://doi.org/10.1016/0016-7037(85)90308-4
- 961 Grossman, J.N., Wasson, J.T., 1982. Evidence for primitive nebular components in
- chondrules from the Chainpur chondrite. Geochim. Cosmochim. Acta 46, 1081–1099.
- 963 https://doi.org/10.1016/0016-7037(82)90061-8
- Guillong, M., Von Quadt, A., Sakata, S., Peytcheva, I., Bachmann, O., 2014. LA-ICP-MS Pb-
- U dating of young zircons from the Kos-Nisyros volcanic centre, SE Aegean arc. J. Anal.
- 966 At. Spectrom. 29, 963–970. https://doi.org/10.1039/c4ja00009a
- Hellmann, J.L., Hopp, T., Burkhardt, C., Kleine, T., 2020. Origin of volatile element
- depletion among carbonaceous chondrites. Earth Planet. Sci. Lett. 549, 116508.
- 969 https://doi.org/10.1016/j.epsl.2020.116508
- Holzheid, A., Lodders, K., 2001. Solubility of copper in silicate as function of oxygen and
- 971 sulfur fugacities teperatures, and silicate composition. Geochim. Cosmochim. Acta 65,
- 972 1933–1951. https://doi.org/10.1016/S0016-7037(01)00545-2
- Holzheid, A., Palme, H., Chakraborty, S., 1997. The activities of NiO, CoO and FeO in
- 974 silicate melts. Chem. Geol. 139, 21–38. https://doi.org/10.1016/S0009-2541(97)00030-2
- Ko, K.Y., Park, J.H., 2011. Dissolution behavior of Indium in CaO-SiO2-Al2O3 slag. Metall.
- 976 Mater. Trans. B Process Metall. Mater. Process. Sci. 42B, 1224–1230.
- 977 https://doi.org/10.1007/s11663-011-9566-6
- Kobertz, D., Müller, M., Molak, A., 2014. Vaporization and caloric studies on lead titanate.
- Calphad Comput. Coupling Phase Diagrams Thermochem. 46, 62–79.
- 980 https://doi.org/10.1016/j.calphad.2014.10.007
- Labrosse, S., Hernlund, J.W., Coltice, N., 2007. A crystallizing dense magma ocean at the
- 982 base of the Earth's mantle. Nature 450, 866–869. https://doi.org/10.1038/nature06355
- Lamoreaux, R.H., Hildenbrand, D.L., Brewer, L., 1987. High-Temperature Vaporization
- Behavior of Oxides II. Oxides of Be, Mg, Ca, Sr, Ba, B, Al, Ga, In, Tl, Si, Ge, Sn, Pb,
- 285 Zn, Cd, and Hg. J. Phys. Chem. Ref. Data 16, 419. https://doi.org/10.1063/1.555799
- Larimer, J.W., 1967. Chemical fractionations in meteorites-I. Condensation of the elements.

- 987 Geochim. Cosmochim. Acta 31, 1215–1238.
- Libourel, G., Portail, M., 2018. Chondrules as direct thermochemical sensors of solar
- protoplanetary disk gas. Sci. Adv. 4. https://doi.org/10.1126/sciadv.aar3321
- 290 Liu, D., Moynier, F., Siebert, J., Sossi, P.A., Hu, Y., Kubik, E., 2022. Origin of moderately
- volatile element depletion on differentiated bodies: Insights from the evaporation of
- indium from silicate melts. Geochim. Cosmochim. Acta 339, 46–57.
- 993 https://doi.org/10.1016/j.gca.2022.09.043
- 994 Lodders, K., 2003. Solar System Abundances and Condensation Temperatures of the
- 995 Elements. Astrophys. J. 591, 1220–1247.
- 996 Mallmann, G., Burnham, A.D., Fonseca, R.O.C., 2021. Mineral- Melt Partitioning of
- 997 Redox- Sensitive Elements, in: Moretti, R., Neuville, D.R. (Eds.), Magma Redox
- Geochemistry, Geophysical Monograph 266. John Wiley & Sons, Inc., pp. 345–367.
- 999 https://doi.org/10.1002/9781119473206.ch17
- Mann, U., Frost, D.J., Rubie, D.C., 2009. Evidence for high-pressure core-mantle
- differentiation from the metal silicate partitioning of lithophile and weakly-siderophile
- elements. Geochim. Cosmochim. Acta 73, 7360–7386.
- 1003 https://doi.org/10.1016/j.gca.2009.08.006
- 1004 Mare, E.R., O'Neill, H.S.C., Berry, A.J., Frigo, C., Glover, C.J., 2021. Coordination change
- of Ge4+ and Ga3+ in silicate melt with pressure. Geochim. Cosmochim. Acta 303, 184–
- 1006 204. https://doi.org/10.1016/j.gca.2021.03.008
- Margrave, J.L., 1967. The Characterization of High Temperature Vapors. John Wiley & Sons,
- New York.
- Mathieu, R., Khedim, H., Libourel, G., Podor, R., Tissandier, L., Deloule, E., Faure, F.,
- Rapin, C., Vilasi, M., 2008. Control of alkali-metal oxide activity in molten silicates. J.
- Non. Cryst. Solids 354, 5079–5083. https://doi.org/10.1016/j.jnoncrysol.2008.07.004
- Mathieu, R., Libourel, G., Deloule, E., Tissandier, L., Rapin, C., Podor, R., 2011. Na2O
- solubility in CaO-MgO-SiO2 melts. Geochim. Cosmochim. Acta 75, 608–628.
- 1014 https://doi.org/10.1016/j.gca.2010.11.001
- Norris, C.A., Wood, B.J., 2017. Earth's volatile contents established by melting and
- vaporization. Nature 549, 507–510. https://doi.org/10.1038/nature23645
- 1017 O'Neill, H.S.C., 2005. A method for controlling alkali-metal oxide activities in one-
- atmosphere experiments and its application to measuring the relative activity coefficients
- of NaO0.5 in silicate melts. Am. Mineral. 90, 497–501.
- 1020 https://doi.org/10.2138/am.2005.1792

- O'Neill, H.S.C., Berry, A.J., Eggins, S., 2008. The solubility and oxidation state of tungsten
- in silicate melts: Implications for the comparative chemistry of W and Mo in planetary
- differentiation processes. Chem. Geol. 255, 346–359.
- https://doi.org/10.1016/j.chemgeo.2008.07.005
- O'Neill, H.S.C., Eggins, S.M., 2002. The effect of melt composition on trace element
- partitioning: an experimental investigation of the activity coefficients of FeO, NiO,
- 1027 CoO, MoO 2 and MoO 3 in silicate melts. Chem. Geol. 186, 151–181.
- O'Neill, H.S.C., Pownceby, M.I., 1993. Thermodynamic data from redox reactions at high
- temperatures. I. An experimental and theoretical assessment of the electrochemical
- method using stabilized zirconia electrolytes, with revised values for the Fe-" FeO",
- 1031 Co–CoO, Ni–NiO and Cu–Cu<sub>2</sub>O. Contrib. to Mineral. Petrol. 114, 296–314.
- Okamoto, H., 1990. The Fe-In (Iron-Indium) system.
- Palme, H., O'Neill, H., 2014. Cosmochemical Estimates of Mantle Composition, in: Holland,
- H.D., Turekian, K.K. (Eds.), Treatise on Geochemistry. Oxford, Elsevier, pp. 1–39.
- 1035 https://doi.org/10.1016/B978-0-08-095975-7.00201-1
- Pankratz, L.B., 1982. Thermodynamic Properties of Elements and Oxides. U.S. Bureau of
- 1037 Mines Bull. 672.
- Paton, C., Hellstrom, J., Paul, B., Woodhead, J., Hergt, J., 2011. Iolite: Freeware for the
- visualisation and processing of mass spectrometric data. J. Anal. At. Spectrom. 26,
- 1040 2508–2518. https://doi.org/10.1039/c1ja10172b
- 1041 Piralla, M., Villeneuve, J., Batanova, V., Jacquet, E., Marrocchi, Y., 2021. Conditions of
- 1042 chondrule formation in ordinary chondrites. Geochim. Cosmochim. Acta 313, 295–312.
- 1043 https://doi.org/10.1016/j.gca.2021.08.007
- 1044 Pretorius, E.B., Muan, A., 1992. Activity-Composition Relations of Chromium Oxide in
- Silicate Melts at 1500°C under Strongly Reducing Conditions. J. Am. Ceram. Soc. 75,
- 1046 1364–1377. https://doi.org/10.1111/j.1151-2916.1992.tb04196.x
- Rammensee, W., Fraser, D.G., 1982. Determination of activities in silicate melts by Knudsen
- 1048 cell mass spectrometry-I. The system NaAlSi3O8-KAlSi3O8. Geochim. Cosmochim.
- 1049 Acta 46, 2269–2278. https://doi.org/10.1016/0016-7037(82)90200-9
- Richter, F.M., Mendybaev, R.A., Christensen, J.N., Ebel, D., Gaffney, A., 2011. Laboratory
- experiments bearing on the origin and evolution of olivine-rich chondrules. Meteorit.
- Planet. Sci. 46, 1152–1178. https://doi.org/10.1111/j.1945-5100.2011.01220.x
- Rubin, A.E., 2000. Petrologic, geochemical and experimental constraints on models of
- chondrule formation. Earth Sci. Rev. 50, 3–27. https://doi.org/10.1016/S0012-

- 1055 8252(99)00067-7
- Ryerson, F.J., 1985. Oxide solution mechanisms in silicate melts: Systematic variations in the
- activity coefficient of SiO2. Geochim. Cosmochim. Acta 49, 637–649.
- 1058 https://doi.org/10.1016/0016-7037(85)90159-0
- Shannon, R.D., 1976. Revised effective ionic radii and systematic studies of interatomic
- distances in halides and chalcogenides. Acta Crystallogr. 32, 751–767.
- Smirnov, A.S., Gribchenkova, N.A., Alikhanyan, A.S., 2021. Vaporization thermodynamics
- of In2O3 by Knudsen effusion mass spectrometry. The standard enthalpy of formation of
- In2O(g). Rapid Commun. Mass Spectrom. 35. https://doi.org/10.1002/rcm.9127
- Sossi, P.A., Fegley, B., 2018. Thermodynamics of Element Volatility and its Application to
- Planetary Processes. Rev. Mineral. Geochemistry 84, 393–459.
- 1066 https://doi.org/10.2138/rmg.2018.84.11
- Sossi, P.A., Klemme, S., O'Neill, H.S.C., Berndt, J., Moynier, F., 2019. Evaporation of
- moderately volatile elements from silicate melts: experiments and theory. Geochim.
- Cosmochim. Acta 260, 204–231. https://doi.org/10.1016/j.gca.2019.06.021
- 1070 Tartèse, R., Sossi, P.A., Moynier, F., 2021. Conditions and extent of volatile loss from the
- Moon during formation of the Procellarum basin. Proc. Natl. Acad. Sci. U. S. A. 118, 1–
- 8. https://doi.org/10.1073/pnas.2023023118
- 1073 Visscher, C., Fegley, B., 2013. Chemistry of impact-generated silicate melt-vapor debris
- 1074 disks. ApJ Lett. 767, L12.
- Wagman, D.D., Evans, W.H., Parker, V.B., Schumm, R.H., Halow, I., Bailey, S.M., Churney,
- 1076 K.L., Nutall, R.L., 1982. The NBS Tables of Chemical Thermodynamic Properties:
- 1077 Reference Data. J. Phys. Chem. 11.
- Wai, C.M., Wasson, J.T., 1977. Nebular condensation of moderately volatile elements and
- their abundances in ordinary chondrites. Earth Planet. Sci. Lett. 36, 1–13.
- 1080 https://doi.org/10.1016/0012-821X(77)90182-0
- Wasson, J.T., 1985. Meteorites: their record of early-system history. W.H. Freeman, New
- 1082 York.
- Wolf, A.S., Jäggi, N., Sossi, P.A., Bower, D.J., 2023. VapoRock: Thermodynamics of
- Vaporized Silicate Melts for Modeling Volcanic Outgassing and Magma Ocean
- 1085 Atmospheres. Astrophys. J. 947, 64. https://doi.org/10.3847/1538-4357/acbcc7
- Wood, B.J., Smythe, D.J., Harrison, T., 2019. The condensation temperatures of the elements:
- 1087 A reappraisal. Am. Mineral. 104, 844–856.
- Wood, B.J., Wade, J., 2013. Activities and volatilities of trace components in silicate melts: a

1089	novel use of metal-silicate partitioning data. Contrib. to Mineral. Petrol. 166, 911-921.
1090	https://doi.org/10.1007/s00410-013-0896-z
1091	Woodhead, J.D., Hellstrom, J., Hergt, J.M., Greig, A., Maas, R., 2007. Isotopic and elemental
1092	imaging of geological materials by laser ablation inductively coupled plasma-mass
1093	spectrometry. Geostand. Geoanalytical Res. 31, 331–343. https://doi.org/10.1111/j.1751-
1094	908X.2007.00104.x
1095	Wu, J., Stebbins, J.F., 2010. Quench rate and temperature effects on boron coordination in
1096	aluminoborosilicate melts. J. Non. Cryst. Solids 356, 2097–2108.
1097	https://doi.org/10.1016/j.jnoncrysol.2010.08.015
1098	Yu, Y., Hewins, R.H., Alexander, C.M.O. 'D., Wang, J., 2003. Experimental study of
1099	evaporation and isotopic mass fractionation of potassium in silicate melts. Geochim.
1100	Cosmochim. Acta 67, 773-786. https://doi.org/10.1016/S0016-7037(02)01176-6
1101	Zinkevich, M., Aldinger, F., 2004. Thermodynamic Assessment of the Gallium-Oxygen
1102	System. J. Am. Ceram. Soc. 87, 683–691. https://doi.org/10.1016/j.jallcom.2006.08.081
1103	